

A p-adic Model of Eternal Inflation, a p-adic Quantum Mechanical Model, and p-adic Anti-de Sitter Space

Brynn Caddel

Contents

1	Introduction	2
1.1	Introduction to p-adic Numbers	3
1.1.1	What Do p-adics Look Like?	3
1.1.2	p-adic Integers and p-adic Numbers	4
1.1.3	Units in \mathbb{Z}_2	7
1.1.4	Aspects of p -adic Norms	7
2	The Eternal Symmetree Model	8
2.1	Eternal Inflation	8
2.1.1	Coloring vacuums and Markov Matrices	10
2.1.2	Imposing Symmetry through Detailed Balance	11
2.1.3	Symmetrizing Markov Matrices	11
2.2	Bruhat-Tits Tree	11
2.2.1	Oriented Tree with Compact Boundary and \mathbb{Z}_p	12
2.2.2	Oriented Tree with Non-Compact Boundary and \mathbb{Q}_p	13
2.3	Correlation Functions	13
2.3.1	Two-Point Correlation Functions	13
2.3.2	Correlators on the Boundary of the Tree	15
2.3.3	Calculating Correlation Functions	15
2.4	Presence of Terminal Vacuums	17
2.4.1	Multifractal Measures	18
2.4.2	Hole Punchers	18
2.4.3	Correlation Functions and Multifractal Measures	19
3	Quantum Mechanical Model of Eternal Symmetree	20
3.1	Physical Models	21
3.2	A Hilbert Space for Observables	22
3.3	Cuntz-Krieger Algebra	23
3.4	Time Evolution in a Quantum Mechanical ES Model	24
3.5	States in a Quantum Mechanical ES Model	24

4	Algebraic Structure of Anti-de Sitter Space	25
4.1	Real Anti de Sitter Space	26
4.1.1	Generators of Flow	26
4.1.2	Lie Derivatives and the Killing Equation	27
4.1.3	Maximally Symmetric Spaces	27
4.1.4	Anti de Sitter Spacetime	30
4.1.5	Transitive $SO(1,2)$ action on AdS_2	31
4.1.6	Constructing AdS_2 as a Coset Space	32
4.2	p -adic Anti de Sitter Space	32
4.2.1	\mathbb{Z} -lattices in \mathbb{R}^2 versus \mathbb{Z}_p -lattices in \mathbb{Q}_p^2	32
4.2.2	Visualizing \mathbb{Q}_p and \mathbb{Q}_p^2	33
4.2.3	Visualizing p -adic Integer Lattices	36
4.2.4	Bruhat-Tits Tree and p -adic Lattices	38
4.2.5	Coordinatizing the Bruhat-Tits Tree	39
4.2.6	Choosing a Gauge	41
4.2.7	Lattices at a Level in the Tree	41
4.2.8	Action of $PGL(2, \mathbb{Z}_2)$ on \mathcal{T}_2	44
4.2.9	Right Multiplication by $PGL(2, \mathbb{Z}_2)$	45
4.2.10	Left Multiplication by $PGL(2, \mathbb{Z}_2)$	45
4.2.11	Constructing the Bruhat-Tits Tree as a Coset Space	47
4.3	\mathcal{T}_2 as a Discrete Analog of AdS_2	47
4.3.1	$SO(2, 1) \approx SL(2, \mathbb{R})$	47
5	Conclusion and Future Work	48
5.1	Conclusion	48
5.2	Future Work	49
5.3	Acknowledgements	50
6	References	50

1 Introduction

Mathematical physics has a steep learning curve since it requires knowledge of both mathematics and physics. It would be nice to tunnel through such a curve, but that may not be an option for non-particle beings. This paper provides an alternative to the quantum tunneling approach for undergraduate students in mathematics who want to study mathematical physics. In particular, we look at models in cosmology, quantum mechanics, and aspects of quantum field theory that make use of the p -adic number system which is studied heavily in areas of number theory.

This paper is not necessarily an introduction to these areas of physics since we focus on specific models, but provides enough examples and introductory explanation to hopefully be helpful to other undergraduates in mathematics.

The p -adic numbers are useful for systems that have an inherently hierarchical structure, such as the Bruhat-Tits tree which is used in the Eternal Symmetree model [2]. This is

a cosmological model for eternal inflation that allows for the construction of multiverses. Chapter 2 of this paper summarizes the results of the Eternal Symmetree model and gives explicit examples of correlation function calculations.

Chapter 3 focuses on making the Eternal Symmetree model a quantum mechanical model. In order to do this, we provide a review of quantum mechanics that makes use of algebras of observables, states, and time evolution operators. The focus on algebras of observables makes this approach differ a bit from a typical physics introduction to quantum mechanics which usually focuses on computing wave equations and understanding Dirac’s bra-ket notation.

In Chapter 4 we focus on a p -adic formulation of AdS/CFT first presented in [14]. In particular, we focus on the analogy between the Bruhat-Tits tree \mathcal{T}_2 and Anti de Sitter Space AdS_2 . In this section we also present a new visualization for p -adic lattices.

1.1 Introduction to p -adic Numbers

1.1.1 What Do p -adics Look Like?

When we write a real number in decimal form, we always have finitely many digits to the left of the decimal point, but may have infinitely many digits to the right of the decimal point.

For example, we can take the rational number $\frac{22}{7}$ and write it in decimal form as

$$3.142857142857\dots = 3.\overline{142857} \in \mathbb{R}$$

where there is a finite number 3 to the left of the decimal point and a recurring sequence of 142857 to the right of the decimal point. Famously, $\frac{22}{7}$ is an approximation for π and it happens to have a recurring fractional sequence. However, π does not have a repeating fractional sequence, but is still in \mathbb{R}

$$\pi = 3.1415926535\dots \in \mathbb{R}.$$

The rational number $\frac{22}{7}$ can also be written in a base 2 as

$$11.001001001\dots = 11.\overline{001} \in \mathbb{R}$$

where there is a finite number of digits to the left of the radix point¹ and a recurring sequence of digits to the right of the radix point.

The importance of these examples is not the recurring sequence of digits to the right of the radix point, but rather the finiteness of the digits to the left of the radix point. This is in contrast to the p -adic numbers which can be thought of as writing out integers in base p , for a prime p , but allowing an infinite number of digits to the left of the radix point and a finite number of digits to the right of the radix point.

In p -adic land, there is a difference between p -adics that have exclusively zeros the right of the radix point and p -adics that have a finite number of digits to the right of the radix

¹The radix point is a generalization of the decimal point which is reserved for numbers written in base 10. Hence the “dec” prefix.

point. The former are p -adic integers \mathbb{Z}_p and the latter are p -adic numbers \mathbb{Q}_p . The following numbers are examples of both p -adic integers and p -adic numbers

$$\begin{aligned}\overline{1234}.0 &= \dots 12341234.0 \in \mathbb{Z}_5 \subset \mathbb{Q}_5, \\ \overline{012210}.0 &= \dots 012210012210.0 \in \mathbb{Z}_3 \subset \mathbb{Q}_3, \\ \overline{110}.11 &= \dots 110110110.11 \in \mathbb{Q}_2, \\ &\dots 345621645210.01 \in \mathbb{Q}_7.\end{aligned}$$

In short, real numbers in decimal form can go on to the right forever and p -adic numbers in decimal form can go on to the left forever.

We formally define the p -adic integers and the p -adic numbers in the next section.

1.1.2 p -adic Integers and p -adic Numbers

For the entirety of this paper, p will be a fixed prime number.

Definition 1.1. A *p -adic integer* is a formal power series

$$\sum_{n \geq 0} a_n p^n \tag{1}$$

with integer coefficients a_n such that $a_n \in \{0, 1, \dots, p-1\}$.

Using this definition, we can identify a p -adic integer $x = \sum_{n \geq 0} a_n p^n$ with the sequence $(a_n)_{n \geq 0}$.

Example 1.1. Take $p = 2$, then

$$29 = \sum_{n \geq 0} a_n 2^n = 1 \cdot 2^0 + 1 \cdot 2^1 + 1 \cdot 2^2 + 0 \cdot 2^3 + 1 \cdot 2^4 + 0 \cdot 2^5 + 0 \cdot 2^6 + 0 \cdot 2^7 \dots$$

where $a_m = 0$ for $m \geq 5$. So we identify the coefficients (a_n) as $(1, 1, 1, 0, 1, 0, 0, 0, \dots)$ and write the 29 as

$$29 = \overline{010111}.0 \tag{2}$$

where we write the recurring zeros as going off to the left since larger powers of 2 are to the left of the radix point.

Let \mathbb{Q} be the field of rational numbers. For every nonzero $x \in \mathbb{Q}$, we can express x as

$$x = \frac{a}{b} \cdot p^u \tag{3}$$

where $u, a \in \mathbb{Z}$ and $b \in \mathbb{Z}^+$ (positive integers) such that a, b are both relatively prime to p ,

$$(p, a) = 1 \text{ and } (p, b) = 1.$$

Definition 1.2. For a nonzero $x \in \mathbb{Q}$ such that (3) holds, the **p -adic norm of x** is defined as

$$|x|_p = \begin{cases} p^{-u} & \text{for } x \neq 0, \\ 0 & \text{for } x = 0 \end{cases}$$

The p -adic norm has the properties:

1. Positivity: $|x|_p \geq 0$ for all $x \in \mathbb{Q}$.
2. Positive Definite: $|x|_p = 0$ if and only if $x = 0$.
3. Multiplicative: $|x \cdot y|_p = |x|_p \cdot |y|_p$ for all $x, y \in \mathbb{Q}$.
4. Triangle Inequality: $|x + y|_p \leq |x|_p + |y|_p$ for all $x, y \in \mathbb{Q}$.
5. Strong Triangle Inequality: $|x|_p$ is a non-Archimedean norm since it satisfies the strong triangle inequality

$$|x + y|_p \leq \max\{|x|_p, |y|_p\}.$$

Example 1.2. Using the multiplicative property of the p -adic norm, we can write a number x satisfying (3) as

$$|x|_p = \left| \frac{a}{b} \cdot p^u \right|_p = p^{-u}.$$

Example 1.3. Here are some examples of 5-adic norms of various values of $x \in \mathbb{Q}$,

$$\begin{aligned} |100|_5 &= |4 \cdot 5^2|_5 = \frac{1}{5^2} = \frac{1}{25}, \\ \left| \frac{4}{1875} \right|_5 &= \left| \frac{4}{3} \cdot 5^{-4} \right|_5 = 5^4 = 625, \\ |3|_5 &= |4|_5 = |7|_5 = \left| \frac{9}{4} \right|_5 = \frac{1}{5^0} = 1. \end{aligned}$$

Theorem 1.1. (Ostrowski) Every non-trivial absolute value on the rational numbers \mathbb{Q} is equivalent to either the usual absolute value or a p -adic absolute value (norm).

A proof for this can be found in [11]. Ostrowski's Theorem implies that the only norms on \mathbb{Q} modulo equivalence are the absolute Euclidean norm, the trivial norm, and a p -adic norms, so there are countably many nontrivial analytic completions with respect to a norm of \mathbb{Q} .

Definition 1.3. The completion of \mathbb{Q} with respect to the p -adic norm defines the p -adic field, also known as the **p -adic numbers**, \mathbb{Q}_p .

This definition implies that any nonzero p -adic number x can be uniquely represented as

$$x = p^{v_p(x)} \sum_{n=0}^{\infty} a_n p^n \tag{4}$$

where $a_0 \neq 0$, $a_n \in \{0, 1, \dots, p-1\}$, and $v_p(x) \in \mathbb{Z}$ is the valuation of x .

The fact that p is prime and not an arbitrary natural number n is important since the p -adic number systems are algebraic fields, while the n -adic number systems are algebraic rings.

A consequence of the n -adic numbers being a ring is that there exist zero divisors in \mathbb{Q}_n . For example, consider the 10-adic numbers. There exists two non-zero elements whose product is zero in the 10-adic numbers:

$$\begin{array}{r} \dots 10112 \\ \times \dots 03125 \\ \hline \dots 00000 \end{array}$$

Since the n -adic numbers have zero divisors, the cancellation law does not always hold.

Since \mathbb{Q}_p is a field, every element has a unique additive inverse. To see why this is true we note that

$$-1 = \frac{p-1}{1-p} = (p-1)(1+p+p^2+\dots) = (p-1) + (p-1)p + (p-1)p^2 \dots$$

and the expression in the last equality takes the form of (4) with $v_p(-1) = 0$ for all $a_m = p-1$. In the third equality, we used the geometric series expansion of $1/(1-p)$. This implies that the multiplication of any $x \in \mathbb{Q}_p$ by -1 gives its unique additive inverse. For various values of p ,

$$-1 = \begin{cases} \overline{1}11.0 & \text{if } p = 2 \\ \overline{2}22.0 & \text{if } p = 3 \\ \overline{6}66.0 & \text{if } p = 7 \end{cases}$$

It can also be shown that there are unique multiplicative inverses for all nonzero $x \in \mathbb{Q}_p$. However, calculating such an inverse by hand can be very tedious, but SageMath software can compute such inverses.

Example 1.4. *In SageMath:*

```
sage : F = Qp(2);
sage : F(6)
2 + 2^2 + O(2^21)
sage : 1/F(6)
2^-1 + 1 + 2^2 + 2^4 + 2^6 + 2^8 + 2^10
+ 2^12 + 2^14 + 2^16 + 2^18 + O(2^19)
```

In the first step, we set $F := \mathbb{Q}_2$. In the second step, we evaluated the base 10 number 6 as a 2-adic number,

$$6 \equiv \overline{0}110.$$

In the third step, we evaluated $\frac{1}{6}$ in \mathbb{Q}_2 . To understand the output, we collect the coefficients of the powers of 2 and write

$$\frac{1}{6} \equiv \dots 0101010101.1 = \overline{01}.1.$$

Therefore, the 2-adic inverse of 6 $\equiv \overline{0110}.0$ is $\overline{01}.1 \in \mathbb{Q}_2$.

1.1.3 Units in \mathbb{Z}_2

We can alternatively define the p -adic integers \mathbb{Z}_p as

$$\mathbb{Z}_p := \{x \in \mathbb{Q}_p \mid |x|_p \leq 1\}. \quad (5)$$

\mathbb{Z}_p is a ring and so we can add and multiply p -adic integers to get new p -adic integers, but multiplicative inverses don't always exist in \mathbb{Z}_p . The subset of \mathbb{Z}_p that does contain inverses for every element is the set of units $\mathbb{U}_p \subset \mathbb{Z}_p$,

$$\mathbb{U}_p := \{x \in \mathbb{Z}_p \mid |x|_p = 1\}. \quad (6)$$

Let's work through an example to see why this is the case.

Example 1.5. Take $p = 2$, then the elements of \mathbb{Z}_2 that contain inverses are those in

$$\mathbb{U}_2 = \{x1.0 \mid x \text{ is an infinite sequence of digits from } \{0, 1\}\}.$$

Some elements in \mathbb{U}_2 are $\overline{1011}.0, \overline{0111}.0, \overline{110001}.0 \in \mathbb{U}_2$. Non-invertible elements in \mathbb{Z}_2 are

$$\mathbb{Z}_2 - \mathbb{U}_2 := \{x0.0 \mid x \text{ is an infinite sequence of digits from } \{0, 1\}\}$$

Some elements in $\mathbb{Z}_2 - \mathbb{U}_2$ are $\overline{010}.0, \overline{1110}.0, \overline{01010}.0 \in \mathbb{Z}_2 - \mathbb{U}_2$.

Let's examine $\overline{010}.0$ to determine why it doesn't have an inverse in \mathbb{Z}_2 . In base 10, $\overline{010}.0$ is 2, which has multiplicative inverse of $\frac{1}{2}$ in base 10. The number $\frac{1}{2}$ as a 2-adic number is 0.1 and so the inverse of $\overline{010}.0$ is $\overline{01}.1 \notin \mathbb{Z}_2$. So $\overline{010}.0$ does have an inverse, it just isn't in \mathbb{Z}_2 .

Note that the numbers in \mathbb{U}_2 happen to be odd numbers in base 10. Numbers not in \mathbb{U}_2 are those that are even numbers in base 10.

1.1.4 Aspects of p -adic Norms

There are a few subtle, but important aspects of p -adic norms that we will discuss in this section. The first of them being how differently values of p can change the p -adic norm of a real number.

For instance, take the number $\frac{112}{2475} = 2^4 \cdot 7 \cdot 3^{-2} \cdot 5^{-2} \cdot 11^{-1}$. Then

$$\left| \frac{112}{2475} \right|_p = \begin{cases} 1/2^4 = 1/16 & \text{if } p = 2, \\ 3^2 = 9 & \text{if } p = 3, \\ 5^2 = 25 & \text{if } p = 5, \\ 1/7 & \text{if } p = 7, \\ 11 & \text{if } p = 11, \\ 1 & \text{if } p \geq 13. \end{cases}$$

We can see a p -adic norm measures the amount to which a number is divisible by p .

The second important aspect of the p -adic norm is how it measures the distance between p -adic numbers. Consider the 5-adic numbers

$$\begin{aligned} a &= \overline{01123423221.0}, \\ b &= \overline{11223423221.0}, \\ c &= \overline{1221.0}. \end{aligned}$$

Evaluating the 5-adic norms gives

$$\begin{aligned} |a - b|_5 &= 5^{-8} = \frac{1}{390,645}, \\ |a - c|_5 &= 5^{-3} = \frac{1}{125}. \end{aligned}$$

Since a and b differ up to the 2^8 position, then a and b are considered to be closer than a and c which only differ up to the 2^3 position.

2 The Eternal Symmetree Model

Now that we have introduced the p -adic numbers, let's examine a cosmological model that utilizes them. In this section we summarize the Eternal Symmetree model presented in [2]. This is a discrete stochastic eternal inflation model that allows for the construction of a multiverse. The symmetry of the Eternal Symmetree model comes from the physical property of detailed balance and the mathematical properties of the Bruhat-Tits tree where the p -adic numbers label the boundary of the tree.

We explicitly compute two-point correlation functions and extrapolated two-point correlation functions, both of which depend on the p -adic norm. These calculations are done without terminal vacuums. Towards the end of this section we discuss how the presence of terminal vacuums leads to multifractal measures on the boundary of the Bruhat-Tits tree. These multifractal measures were first introduced in [3]. We then compute two-point extrapolated correlation functions for a tree which contains terminal vacuums.

2.1 Eternal Inflation

The universe went under a period of rapidly accelerating expansion. After this rapid expansion, inflation stopped and vacuum energies decayed and produced all of the cosmic structures present in our universe today. Models that propose that inflation stopped all of a sudden and uniformly are known as *inflation* models. The goal of such models is to describe why the universe is flat and homogeneous.

Eternal inflation is similar to inflation in that it still postulates that the early universe was dominated by a period of exponential growth where this growth eventually stopped and was converted to matter and radiation. However, in eternal inflation, this growth doesn't have to stop in all regions of space. Bubbles of space could have stopped inflating or fallen onto trajectories where inflation ends. If the universe was not expanding, then each bubble

would eventually run into another bubble and the entire universe would be converted to a lower vacuum energy. However, if the universe were rapidly expanding, the the space between bubbles is growing as the bubbles themselves are growing. If expansion is fast enough, then the growth of inflating space will be faster than its conversion into lower energy bubbles. Thus, Eternal inflation is a theory of many bubble universes nucleating and growing inside an expanding background multiverse.

Consider a model with potential energy $V(\phi)$ as a function of a single scalar field ϕ with a barrier and two or more local minima Fig. 1.

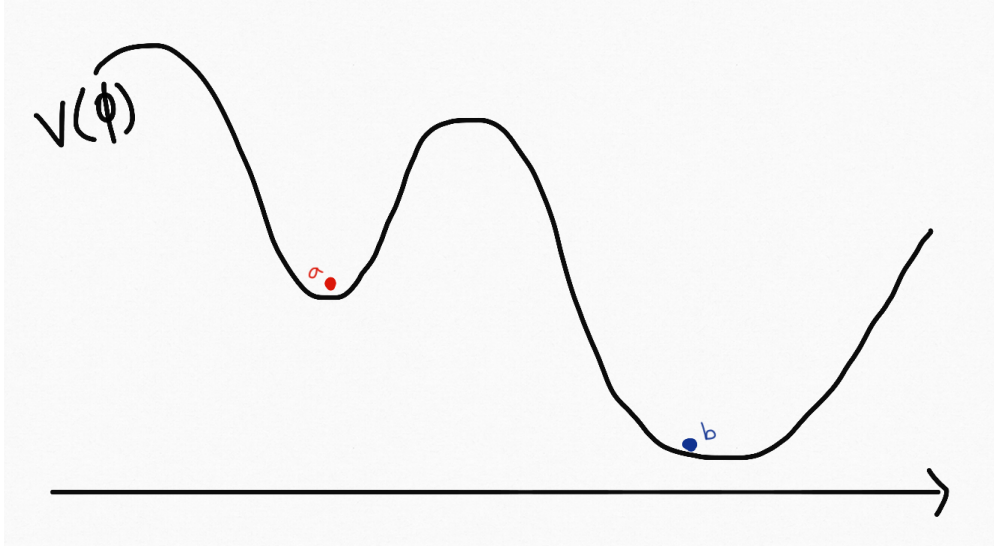


Figure 1: Potential energy $V(\phi)$ with a barrier and two local minima.

If the field is in the minimum, then in classical mechanics, the field will stay there forever. However, quantum mechanically, the field can tunnel across the barrier. This quantum tunneling is where the bubble universes begins. The field will then begin a slow roll down the potential.

Solutions to Einstein's Equations

$$R_{ij} - \frac{1}{2}Rg_{ij} + \Lambda g_{ij} = \kappa T_{ij}$$

at any one of these minima is de Sitter space (dS). De Sitter space is a maximally symmetric space with constant positive scalar curvature. It is characterized by the radius of curvature R .

Consider a causal patch of de Sitter space. These causal patches are regions of spacetime and so we can foliate spacetime by spacelike sections. As time goes forward, the number of causal patches replicate and these causal patches then grow exponentially with time. The exact number of causal patches produced depends on the dimension of the system. In $d = 3$, there will be 2^3 causal patches produced. In general, there will be 2^d causal patches produced. This replication of causal patches is very important to Eternal Inflation since we can think of causal patches as defining lattices spacing [12]. These lattices spacings in turn define a *cell size* on a surface. This suggests that we should think of inflating spaces as lattice systems

where the numbers of lattice point replicates. In $d = 2$, each 2-folding replicates the number of causal patches and therefore replicated the number of lattices sites.

2.1.1 Coloring vacuums and Markov Matrices

The Eternal Symmetree (ES) model [2] is a variation of the generalized Mandelbrot percolation model of eternal inflation. This model is a stochastic one which begins with a discrete collection of vacuums indexed by the color of the vacuum n .

Each vacuum has a cosmological constant Λ , which is the value of the energy density of the vacuum space and is proportional to the square of its Hubble expansion rate H_n . We will work with an entropy $S_n \sim \frac{1}{H_n^2 G}$, which counts the number of microstates that form a single macroscopic state n .

We begin with a vacuum of color n , then allow bubbles to nucleate from this initial vacuum. The rate of nucleation of bubbles of type n in a vacuum of type m is represented by γ_{mn} . The order of the indices of γ_{mn} are important here since, in general, $\gamma_{mn} \neq \gamma_{nm}$. After u stochastic processes, the probability that a vacuum is the color n is given by

$$P_n(u) := \frac{N_n(u)}{N(u)} \quad (7)$$

where $N(u)$ is the total number of coloring outcomes and $N_n(u)$ is the number of vertices of color n .

We will use Markov matrices to represent the probability of transitioning between different colors of vacuums. This Markov matrix is a matrix for a linear operator in a particular basis which we will call the *color basis*. We can also compute the components of this Markov matrix in a different basis.

The following Markov matrix says that the probability of transitioning from colors red r to blue b is 0.2, while that probability of remaining in a blue state after one step is 0.6,

$$\begin{array}{c} r \quad b \\ r \quad \begin{pmatrix} .8 & .2 \\ .4 & .6 \end{pmatrix}. \\ b \end{array}$$

Since the entries in a Markov matrix represent probabilities, each entry must be a nonnegative real number. Additionally, all the rows in a Markov matrix must sum to 1.

The probabilities $P_n(u)$ from (7) are determined by the following rate equations that describe the step u to $u + 1$,

$$P_m(u + 1) = P_m(u) - \sum_n \gamma_{nm} P_m(u) + \sum_n \gamma_{mn} P_n(u). \quad (8)$$

The term $\sum_n \gamma_{nm} P_m(u)$ represents the depletion of the m^{th} color by transitions to other colors. The term $\sum_n \gamma_{mn} P_n(u)$ represents the increase due to transitions from other colors. We can compactly write these rate equations as

$$P_m(u + 1) = G_{mn} P_n(u) \quad (9)$$

where $G_{mn} := \delta_{mn} - \gamma_{pm} \delta_{mn} + \gamma_{mn}$.

2.1.2 Imposing Symmetry through Detailed Balance

When examining the transitions between microscopic states, which is described in our case by the coloring of vertices, *detailed balance* states that the transition rate is larger in the direction that increases the number of microstates:

$$\gamma_{nm}e^{S_m} = \gamma_{mn}e^{S_n} \quad (10)$$

In probability theory, this is called a *reversible Markov chain*.

The statement of detailed balance (10) can be written in terms of a real symmetric matrix M as

$$\gamma_{mn} = M_{mn}e^{S_m}.$$

However, the matrix G from (9) is not always a symmetric matrix. In general, an arbitrary Markov matrix will not be symmetric. So in order to proceed, we introduce a method of symmetrizing any Markov matrix.

2.1.3 Symmetrizing Markov Matrices

We begin with a non-symmetric Markov matrix G_{mn} and define the following matrices

$$Z_{mn} := \delta_{mn}e^{S_n/2} \quad \text{and} \quad S_{mn} := Z^{-1}GZ. \quad (11)$$

where S will be a symmetric matrix. The values for S_n need be chosen appropriately. For example, in a general 2×2 case, with the Markov matrix

$$G = \begin{pmatrix} g_{11} & g_{12} \\ g_{21} & g_{22} \end{pmatrix}$$

choose $S_1 = \ln(g_{12})$ and $S_2 = \ln(g_{21})$. This new matrix S will be symmetric. To see why the resulting matrix S is symmetric, consider the following example.

Example 2.1. *Let G be the Markov matrix*

$$\begin{pmatrix} .6 & .4 \\ .3 & .7 \end{pmatrix} \quad (12)$$

and let $S_1 = \ln(.4)$ and $S_2 = \ln(.3)$, then

$$Z^{-1}GZ = \begin{pmatrix} \frac{1}{\sqrt{.4}} & 0 \\ 0 & \frac{1}{\sqrt{.3}} \end{pmatrix} \begin{pmatrix} .6 & .4 \\ .3 & .7 \end{pmatrix} \begin{pmatrix} \sqrt{.4} & 0 \\ 0 & \sqrt{.3} \end{pmatrix} = \begin{pmatrix} .6 & \sqrt{.4}\sqrt{.3} \\ \sqrt{.4}\sqrt{.3} & .7 \end{pmatrix} = S. \quad (13)$$

2.2 Bruhat-Tits Tree

In the previous sections, we discussed the implications of eternal inflation and how the ES model sets out to describe this type of inflation through the coloring of vertices which represent the various microstates, along with the notion of detailed balance which describes these transitions as being a statistical process. In the following section, we will look at the geometry of the tree graph and see how it gives us a visual interpretation for this bubble nucleation process.

2.2.1 Oriented Tree with Compact Boundary and \mathbb{Z}_p

Let's begin by considering the directed rooted tree with 2 branchings from each vertex which grows out of a single branch. For this case, we will use base 2 numbers to represent vertices in the tree and the 2-adic integers \mathbb{Z}_2 to label points on the boundary as seen in Fig. ??.

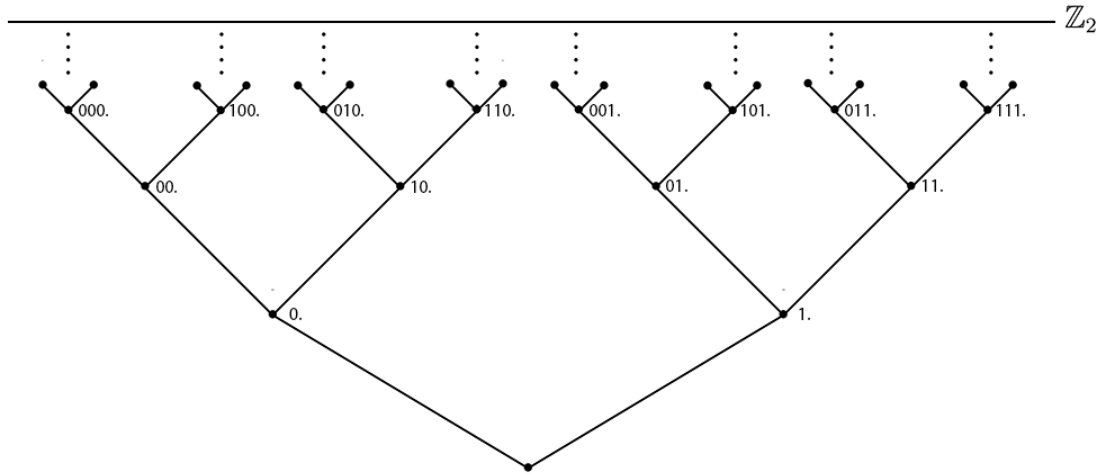


Figure 2: A 2-adic tree with boundary \mathbb{Z}_2 .

For a general case, numbers in base p would represent vertices within the tree and those on the boundary would be expressed by the p -adic numbers \mathbb{Z}_p . Begin constructing the tree by starting at the radix point and working to the left. Each added digit corresponds to moving up from one vertex to another in one successive step. We will refer to the different levels, or steps taken up the tree, by an index u which is depicted in ??

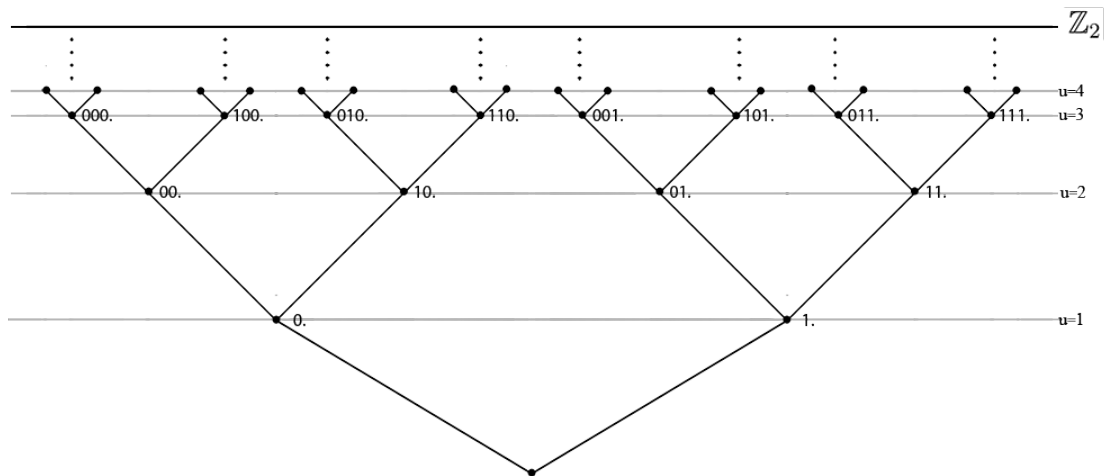


Figure 3: A 2-adic tree with boundary \mathbb{Z}_2 with levels denoted by u .

Any point in the tree is a finite ordinary integer, for example,

$$101110001.$$

which is binary for 369 in base 10. This, however, is not a number in \mathbb{Z}_2 because it is a finite string of digits. The 2-adic integers are unending to the left, so

$$\overline{11011001}.$$

is an example of a point on the boundary of the tree.

Since we are interested in this branching process as it tends to infinity, we introduce a cutoff point u_f that will work as a bound for u . Thus, we can define the p -adic integers on the boundary of the tree by letting $u_f \rightarrow \infty$. For each point a in the tree, there will be a corresponding set of points on the boundary that are in the causal future of a , namely

$$\{\text{descendants of } a\} := \{x \in \mathbb{Z}_2 \mid x = \dots x_2 x_1 x_0 a. \text{ and } x_i \in \{0, 1\}\}$$

The boundary described above is the compact version of the ES model because the space \mathbb{Z}_p of p -adic integers is a compact space [10]. For the non-compact case, we need to generalize our number system to the p -adic numbers \mathbb{Q}_p .

2.2.2 Oriented Tree with Non-Compact Boundary and \mathbb{Q}_p

The construction of the non-compact tree will be very similar to the one described in the previous section, where the main difference between the compact and non-compact cases comes from the p -adic numbers being defined by allowing there to be a finite number of digits to the right of the radix point. For example,

$$\overline{101001101}.1011 \in \mathbb{Q}_2.$$

The p -adic numbers allows us to think of the tree as one that extends into the infinite past. We can do this by selecting a cutoff point u_1 and letting it tends towards $-\infty$.

2.3 Correlation Functions

2.3.1 Two-Point Correlation Functions

When calculating these correlation functions, we assume that detailed balance is satisfied and so we write

$$G_{mn} = e^{S_m/2} S_{mn} e^{-S_n/2}. \quad (14)$$

The equation above describes the components of G and S in the color basis ($|m\rangle$).

Since S is symmetric, we can diagonalize it with an ordered basis ($|I\rangle$) of N orthonormal eigenvectors of S where N is the number of colors. The corresponding eigenvalues are λ_I , so

$$S|I\rangle = \lambda_I|I\rangle, \quad \langle I|J\rangle = \delta_{IJ}, \quad \text{and } S = \sum_I \lambda_I |I\rangle \langle I|. \quad (15)$$

In terms of these two bases,

$$G_{mn} = e^{m/2} \langle m | \sum_I \lambda_I |I\rangle \langle I | n \rangle e^{-n/2}.$$

Definition 2.1. The vertex a at time u_i be color m . A **propagator** is the probability that a descendant of a will be the color n at time u_f , denoted as $P_{mn}(u)$ where $u = u_f - u_i$.

This probability can be expressed as the u -th power of the Markov matrix G ,

$$P_{mn}(u) := (G^u)_{mn} = e^{m/2} (S^u)_{mn} e^{-n/2} = \langle m | \sum_I \lambda_I^u | I \rangle \langle I | e^{\frac{S_m - S_n}{2}} | n \rangle. \quad (16)$$

Now let's consider the correlation function for vertices a and b at the cutoff point u_f .

Definition 2.2. Let a and b be vertices at time u_f . The **correlation function** $C_{mn}(a, b)$ is the joint probability that vertex a has color m and vertex b has color n .

By looking at the causal pasts of both a and b , we can find the first common ancestor vertex c . Let's say this happens at time u_i and the color of the ancestor vertex is r . The joint probability for a and b to have colors m and n is

$$P_{mr}(u_f - u_i) P_{nr}(u_f - u_i). \quad (17)$$

We multiply the correlation function by the normalized fixed point probability $P_n^{\{0\}} = \frac{e^{S_n}}{\sum_m e^{S_m}}$ to study the system in equilibrium. Setting the normalizing factor $\mathcal{N} := \sum_m e^{S_m}$, the correlation function is

$$C_{mn}(a, b) = \frac{1}{\mathcal{N}} \sum_r e^{S_r} P_{mr}(u_f - u_i) P_{nr}(u_f - u_i). \quad (18)$$

Using (16), the propagators in the correlation function results in

$$C_{mn}(a, b) = \frac{1}{\mathcal{N}} \sum_{I, J, r} e^{S_r} \left(\lambda_I^{u_f - u_i} \langle m | | I \rangle \langle I | | r \rangle e^{\frac{S_m - S_r}{2}} \right) \left(\lambda_J^{u_f - u_i} \langle n | | J \rangle \langle J | | r \rangle e^{\frac{S_n - S_r}{2}} \right) \quad (19)$$

$$= \frac{1}{\mathcal{N}} \sum_{I, J, r} \left(\lambda_I^{u_f - u_i} \langle m | | I \rangle \langle I | | r \rangle e^{\frac{S_m}{2}} \right) \left(\lambda_J^{u_f - u_i} \langle n | | J \rangle \langle J | | r \rangle e^{\frac{S_n}{2}} \right) \quad (20)$$

$$= \frac{1}{\mathcal{N}} \sum_{I, J, r} \lambda_I^{u_f - u_i} \lambda_J^{u_f - u_i} \langle m | | I \rangle \langle I | | r \rangle \langle r | | J \rangle \langle J | | n \rangle e^{\frac{S_m + S_n}{2}} \quad (21)$$

$$= \frac{1}{\mathcal{N}} \sum_{I, J} \lambda_I^{u_f - u_i} \lambda_J^{u_f - u_i} \langle m | | I \rangle \langle I | | J \rangle \langle J | | n \rangle e^{\frac{S_m + S_n}{2}} \quad (22)$$

$$= \frac{1}{\mathcal{N}} \sum_{I, J} \lambda_I^{u_f - u_i} \lambda_J^{u_f - u_i} \langle m | | I \rangle \delta_{IJ} \langle J | | n \rangle e^{\frac{S_m + S_n}{2}} \quad (23)$$

using the orthonormality of these eigenvectors;

$$C_{mn}(a, b) = \frac{1}{\mathcal{N}} \sum_I \lambda_I^{2(u_f - u_i)} \langle m | | I \rangle \langle I | | n \rangle e^{\frac{S_m + S_n}{2}}. \quad (24)$$

Following [2] we define

$$C_{IJ}(a, b) := \mathcal{N} e^{-\frac{S_m - S_n}{2}} C_{mn}(a, b) = |I\rangle \langle J| (\lambda_I)^{2(u_f - u_i)} = (\lambda_I)^{2(u_f - u_i)} \delta_{IJ} \quad (25)$$

where δ_{IJ} is the Kronecker delta.

For the case where $N = 2$, in other words a 2×2 Markov matrices, the two-point correlation function are used to characterize the probability of transitioning between colors while stepping up the tree, this correlation function $C_{IJ}(a, b)$ amounts to the matrix $(\lambda_I)^{2(u_f - u_i)} \delta_{IJ}$,

$$C(a, b) = \begin{pmatrix} \lambda_1^{2(u_f - u_i)} & 0 \\ 0 & \lambda_2^{2(u_f - u_i)} \end{pmatrix}$$

in the eigenbasis where λ_1 and λ_2 are the eigenvalues for the eigenvectors $|1\rangle$ and $|2\rangle$, respectively.

2.3.2 Correlators on the Boundary of the Tree

Let's allow the cutoff point u_f tend to infinity to examine how the probability of transitioning between colors changes at the future boundary. To do this, we define a sequence $\{a_{u_f}\}$ and $\{b_{u_f}\}$ in the causal futures of a and b , respectively. As $u_f \rightarrow \infty$, these sequences will define p -adic numbers x and y . To ensure that our results are finite, we multiply by a wave function renormalization factor [2] of $\lambda_I^{-u_f}$ to each external leg.

$$\langle \mathcal{O}_I(x) \mathcal{O}_J(y) \rangle := \lim_{u_f \rightarrow \infty} C_{IJ}(a_{u_f}, b_{u_f}) \lambda_I^{-u_f} \lambda_J^{-u_f}. \quad (26)$$

The extrapolated correlation function becomes

$$\langle \mathcal{O}_I(x) \mathcal{O}_J(y) \rangle = \lim_{u_f \rightarrow \infty} \delta_{IJ} \lambda_I^{2(u_f - u_i)} \lambda_I^{-u_f} \lambda_J^{-u_f} = \delta_{IJ} \lambda_I^{-2u_i}. \quad (27)$$

Since $\lambda_I \in \mathbb{R}$ and the p -adic distance $|x - y|_p$ is p^{-u_i} , the extrapolated correlation function can be written as

$$\langle \mathcal{O}_I(x) \mathcal{O}_J(y) \rangle = \frac{\delta_{IJ}}{|x - y|_p^{2\Delta_I}}. \quad (28)$$

So we can see that there is a simple relation between scattering in the bulk of the tree and correlators on the boundary of the tree. Higher point correlation functions are described in [2].

2.3.3 Calculating Correlation Functions

Let's work through a concrete example to see how these correlation functions can be calculated and how the p -adic distance plays such an important role in these computations.

Recall from (27) that the Markov matrix

$$G = \begin{pmatrix} .6 & .4 \\ .3 & .7 \end{pmatrix}$$

can be symmetrized through a similarity transform, as in (13). The resulting symmetric matrix, which has eigenvalues $\lambda_1 = 1$ and $\lambda_2 \approx 0.3$, is

$$S = \begin{pmatrix} .6 & \sqrt{.4}\sqrt{.3} \\ \sqrt{.4}\sqrt{.3} & .7 \end{pmatrix}.$$

Next, we choose vertices a and b in the tree at the same time $u_f = 6$,

$$a = 101110.0 \text{ and } b = 010010.0$$

where these integers are represented in base two since the future boundary is \mathbb{Q}_2 .

Tracing back the causal pasts of both vertices, we find their first common ancestor is $r = 10.0$ which occurs at time $u_i = 2$. The extrapolated correlation function in the I, J basis is

$$C_{IJ}(101110.0, 010010.0) = |I\rangle \langle J| \lambda_I^{2(6-2)} = \delta_{IJ} \lambda_I^8.$$

Since the eigenvalues of S are $\lambda_1 = 1$ and $\lambda_2 \approx 0.3$, the resulting matrix becomes

$$C(101110.0, 010010.0) = \begin{pmatrix} 1^8 & 0 \\ 0 & 0.3^8 \end{pmatrix}.$$

By the Perron-Frobenius theorem, the largest eigenvalue of any $n \times n$ Markov matrix will always be 1 and every other eigenvalue will be strictly less than 1. This means that as we raise any Markov matrix to larger powers, the eigenvalues strictly less than 1 tend towards zero. Notice that $0.3^8 = 0.00006561$ is already a small number. Thus, the transient behavior of the system is determined by the eigenvalues of S which are all less than 1 in magnitude.

To see this transient behavior take place, we calculate the extrapolated correlators. Let

$$\begin{aligned} x &= \overline{11}101110.0, \\ y &= \overline{01}010010.0. \end{aligned}$$

be the p -adic numbers defined by the sequences $a_{u_f} = 1111101110.0$ and $b_{u_f} = 0101010010.0$. Then the extrapolated correlators multiplied by the wave function renormalization factors $\lambda_I^{-u_f}$ is

$$\langle \mathcal{O}_I(\overline{11}101110.0) \mathcal{O}_J(\overline{01}010010.0) \rangle = \lim_{u_f \rightarrow \infty} C_{IJ}(a_{u_f}, b_{u_f}) \lambda_I^{-u_f} \lambda_J^{-u_f}$$

Then by (27),

$$\lim_{u_f \rightarrow \infty} \delta_{IJ} \lambda_I^{2(u_f-2)} \lambda_I^{-u_f} \lambda_J^{-u_f} = \delta_{IJ} \lambda_I^{-2(2)} = \delta_{IJ} 2^{-4}$$

since $\lambda_I = p^{-\Delta_I} = 2^{-\Delta_I}$.

From here it can be seen that $\delta_{IJ}2^{-2(2)} = \frac{\delta_{IJ}}{|x-y|_2^{2\Delta_I}}$ because the p -adic distance between x and y is

$$|\overline{11101110.0} - \overline{01010010.0}|_2 = 2^{-2}.$$

Therefore,

$$\langle \mathcal{O}_2(\overline{11101110.0}) \mathcal{O}_2(\overline{01010010.0}) \rangle = \frac{\delta_{IJ}}{|\overline{11101110.0} - \overline{01010010.0}|_2^{-2\log(.3)}}$$

since $\lambda_2 = .3 = 2^{-\Delta_2} \iff \Delta_2 = -\log_2(.3)$.

2.4 Presence of Terminal Vacuums

So far in our discussion of the ES model, we have only considered cases where no limitation has been placed on the future-pointing direction of transitions between vacuums. However, terminal vacuums, those from which no further transition between vacuums is possible, are an essential aspect of eternal inflation [5] and so we would like to create a mechanism for modeling them. This is done by associating a terminal vacuum with a vertex on the tree graph from which no further branching occurs. These portions of the tree are referred to as pruned branches.

Consider the vertex 0200.02 in the tree \mathcal{T} with $\mathbf{P} = \{0, 1, 2\}$ and suppose that this is a terminal vacuum, so no further branching from this point is allowed. In other words, the vertices

$$00200.02 \text{ and } 20200.02$$

will not appear in the tree, while

$$10200.02$$

will persist to the future boundary as a single lineage. Consequently, the future boundary $\partial\mathcal{T}$ of the tree is modified by pruning to $\mathbb{Q}_3 - \{x0200.02 \mid x = \dots a_2 a_1 a_0, (\exists i \in \mathbb{N}) A_{a_i a_{i+1}} = 0\}$.

The pruning of the branch 1211.12 was an example of pruning in one place on the tree, but we may require that all future branchings in one direction, say the middle vertex be disallowed. To do this, consider an incidence matrix A with entries in $\{0, 1\}$ such that in each row and column there is at least one entry equal to one. This incidence matrix A describes the directions in which vacuums may transition in the future direction.

As an example, take the incidence matrix

$$\begin{matrix} & 0 & 1 & 2 \\ 0 & \begin{pmatrix} 1 & 0 & 1 \end{pmatrix} \\ 1 & \begin{pmatrix} 0 & 1 & 0 \end{pmatrix} \\ 2 & \begin{pmatrix} 1 & 0 & 1 \end{pmatrix} \end{matrix}$$

where 0, 1, 2 along the rows and columns represent the elements in $\mathbf{P} = \{0, 1, 2\}$. If the stochastic transition process begins in state $|1\rangle$, then transitioning to state $|0\rangle$ and $|2\rangle$ is disallowed by this incidence matrix. The corresponding tree graph will be pruned at each level in the middle vertex.

The bulk of the tree can be described by

$$\mathcal{T}_A := \{a_{n-1} \dots a_1 a_0 . b_0 \dots b_n \mid A_{a_k a_{k+1}} = 1, k = 0, 1, \dots, n-1, n \in \mathbb{N}\}$$

$a_i, b_j \in \mathbf{P}$. The subscript A refers to the admissible matrix used to prune the tree.

Since the boundary of the pruned tree is subset of \mathbb{Q}_p , we would like language that reflects that subset nature. So we define admissible numbers as follows.

Definition 2.3. *The **admissible numbers** of \mathbb{Q}_p with respect to A are the elements of $\partial\mathcal{T}_A$,*

$$\partial\mathcal{T}_A := \{\dots a_2 a_1 a_0 . b_0 \dots b_n \mid A_{a_k a_{k+1}} = 1\} \subseteq \mathbb{Q}_p$$

where $a_i, b_j \in \mathbf{P}$ where the subscript A denotes the incidence matrix A that modified the tree \mathcal{T} to the pruned tree \mathcal{T}_A .

If a number is not in \mathcal{T}_A , then it is not considered an admissible number and does not appear on the future boundary of the tree. Thus, any ray in the tree that contains a non-admissible consecutive pair of edges $a_k a_{k+1}$ is pruned.

Now that we have discussed a mechanism for pruning the tree, we would like to compute correlation functions to see how these calculations differ from the unpruned correlation functions.

2.4.1 Multifractal Measures

As this pruning process continues, the tree will begin to display fractal-like behavior. The future boundary of the tree will indeed have a multifractal structure that we can examine using the following self-similar measures [3].

Let A be an incidence matrix with Perron-Frobenius (PF) eigenvalue λ_A and corresponding eigenvector v_A . The measure $\mu : \partial\mathcal{T}_A \rightarrow \mathbb{R}$ such that

$$\mu(\partial\mathcal{T}(\alpha))_{\alpha_k} = \lambda_A^{-k} (v_A)_{\alpha_k} \quad (29)$$

where α_k denotes the k^{th} component of the PF eigenvector and a vertex $\alpha \in \mathcal{T}_A$ of length k , $\alpha = \alpha_1 \alpha_2 \dots \alpha_k$ defines a multifractal measure on the future boundary. This measure satisfies the self-similarity condition

$$\mu = \lambda_A^{-1} \sum_{\alpha \in \mathbf{P}} \mu \circ \sigma_\alpha^{-1} \quad (30)$$

and has Hausdorff dimension $\delta_A = \log(\lambda_A) / \log(|\mathbf{P}|)$ [3].

2.4.2 Hole Punchers

Just as in prior calculations, we begin with a Markov matrix G ,

$$G = \frac{1}{20} \begin{pmatrix} 7 & 1 & 12 \\ 1 & 15 & 4 \\ 3 & 1 & 16 \end{pmatrix} \quad (31)$$

and obtain a symmetric matrix from G by a similarity transform $ZGZ^{-1} = S$,

$$\frac{1}{20} \begin{pmatrix} 4 & 0 & 0 \\ 0 & 4 & 0 \\ 0 & 0 & 8 \end{pmatrix} \begin{pmatrix} 7 & 1 & 12 \\ 1 & 15 & 4 \\ 3 & 1 & 16 \end{pmatrix} \begin{pmatrix} 4 & 0 & 0 \\ 0 & 4 & 0 \\ 0 & 0 & 8 \end{pmatrix}^{-1} = \frac{1}{20} \begin{pmatrix} 7 & 1 & 6 \\ 1 & 15 & 2 \\ 6 & 2 & 16 \end{pmatrix} \quad (32)$$

Now let's define a transition matrix A ,

$$A = \begin{pmatrix} 1 & 0 & 1 \\ 0 & 1 & 0 \\ 1 & 0 & 1 \end{pmatrix} \quad (33)$$

and use it to prune the tree. If a vertex begins in state 1, it must remain in state 1. If a vertex begins in state 0, then it can only stay in 0 or transition to state 2. This process continues each step up the tree and the resulting future boundary will resemble that of the Cantor set.

At this point, we have defined two separate matrices, G and A . The stochastic properties of G assign probabilities of transitioning between states, while the matrix A tells us the directions in which we can transition. Let's now define a matrix X ,

$$X := A \cdot S = \frac{1}{20} \begin{pmatrix} 1 & 0 & 1 \\ 0 & 1 & 0 \\ 1 & 0 & 1 \end{pmatrix} \cdot \begin{pmatrix} 7 & 1 & 6 \\ 1 & 15 & 2 \\ 6 & 2 & 16 \end{pmatrix} = \frac{1}{20} \begin{pmatrix} 7 & 0 & 6 \\ 0 & 15 & 0 \\ 6 & 0 & 16 \end{pmatrix} \quad (34)$$

where \cdot denotes the *hole punching product*, which is essentially entry-wise multiplication, but since the zeros in A cause the resulting matrix X to also have zeros in it, A has the effect of ‘‘punching holes’’ in the matrix G . This new matrix X attempts to encapsulate the properties of both G and A , but falls short of doing so because X is not Markov and does not have a Perron-Frobenius eigenvalue of 1, instead having largest eigenvalue $\lambda = 19/20$. In fact, for any transition matrix A and any Markov matrix G , the hole punched product of these matrices will have a Perron-Frobenius eigenvalue $\lambda < 1$.

2.4.3 Correlation Functions and Multifractal Measures

The self-similar measure

$$\mu(\partial\mathcal{T}_A(\alpha)) = \lambda_A^{-k} v_A \quad (35)$$

was first presented in [3], where λ_A is the Perron-Frobenius eigenvalue of A and α is an admissible word of length k . This is a fractal measure with Hausdorff dimension

$$\delta_A = \frac{\log(\lambda_A)}{\log(\mathbf{P})} = \frac{1}{3} \log(2) = \dim_H(\partial\mathcal{T}_A).$$

The correlation function with multifractal measure in the color basis is

$$C(a, b) = \frac{1}{\mathcal{N}\mathcal{N}\lambda_X^k} \sum_I \lambda_I^{2(u_f - u_i)} |I\rangle \langle I| e^{\frac{S_m - S_n}{2}} \quad (36)$$

and the the correlation function with multifractal measure is in the eigenbasis is

$$C_{IJ}(a, b) = \frac{1}{N\lambda_X^k} \delta_{IJ} \lambda_I^{2(u_f - u_i)}. \quad (37)$$

where N is the number of colors and we used (25) to go from the second to third equation. Note that λ_X in the denominator, rather than the numerator because the volume measure of the future boundary with respect to the measure remains normalized on a fractal that scales as the size of a power of λ_X .

Example 2.2. We choose the Markov matrix

$$G = \frac{1}{20} \begin{pmatrix} 7 & 1 & 12 \\ 1 & 15 & 4 \\ 3 & 1 & 16 \end{pmatrix}$$

and symmetrize it using (32) and then take the hole punching product as in (34). The eigenvalues of the symmetrized and hole-punched matrix are

$$\lambda_1 = \frac{19}{20}, \quad \lambda_2 = \frac{3}{4}, \quad \lambda_3 = \frac{1}{5}.$$

The admissibility matrix we are using is

$$A = \begin{pmatrix} 1 & 0 & 1 \\ 0 & 1 & 0 \\ 1 & 0 & 1 \end{pmatrix}.$$

An admissible number with respect to this admissibility matrix A is $\alpha = 02202$ which has length $k = 5$. Using the self-similar measure from (35),

$$\mu(\partial\mathcal{T}_A(02202)) = \lambda_A^{-k} v_A = \frac{1}{25} v_A. \quad (38)$$

We now compute a two-point correlation function between points in the tree using $\mathbf{P} = \{0, 1, 2\}$. Choose $a = 101110.0$ and $b = 010010.0$, then the most recent common ancestor of a and b is at $u = 2$. This means that $u_f - u_i = 6 - 2 = 4$.

$$C_{X,k}(101110.0, 010010.0) = \frac{1}{N\lambda_X^k} \lambda_I^{2(u_f - u_i)} \delta_{IJ} = \frac{1}{(3)\left(\frac{19}{20}\right)^5} \begin{pmatrix} \left(\frac{19}{20}\right)^8 & 0 & 0 \\ 0 & \left(\frac{3}{4}\right)^8 & 0 \\ 0 & 0 & \left(\frac{1}{5}\right)^8 \end{pmatrix}$$

where the subscript X denotes the symmetrized, hole punched matrix as in (34). The subscript k denotes the admissible number used. The number of colors is $N = 3$ since we are working with $\mathbf{P} = \{0, 1, 2\}$.

3 Quantum Mechanical Model of Eternal Symmetree

In order to quantize the Eternal Symmetree model, we need to first have an idea of what a quantum mechanical system is and how it differs from a classical mechanical system. To do this, we will present a mathematical framework for *any* model of a physical system and then highlight the differences between classical and quantum mechanical models.

3.1 Physical Models

One of the first specifications of a physical system is to define a set of *observables*, which are representations of measurable physical quantities [6]. Examples of such physical observables would be the position and momentum of an airborne cannonball or a photon being emitted from the Sun. Regardless of whether we are considering classical mechanics (CM) or quantum mechanics (QM), these observables are represented by bounded, self-adjoint linear operators that reside in a Hilbert space. These same observables also generate a C^* -algebra \mathcal{A} that is referred to as an *algebra of observables*.

Another ingredient for models of physical systems are *states* of the system. For each observable a , there is an expected value of that observable $\phi(a)$. We require that for all observables $a \in \mathcal{A}$ the expectation value of a positive operator is positive,

$$\phi(a^*a) \geq 0$$

and also require that the expectation value of the identity is the identity,

$$\phi(1) = 1.$$

This makes sense from an experimental viewpoint because if we choose a coordinate system and then want to measure the momentum of a forward-moving particle, we would expect to measure a positive quantity rather than a negative quantity. Similarly, if we measure the position of a stationary particle, then we would expect to measure the identity operator since the particle didn't move.

Finally, physical systems should be endowed with a notion of time evolution [6] which characterizes the change of a state brought about by the passage of time. To make this abstract operator compatible with experiments, we place a composition requirement on our time evolution α such that for any times $s, t \in \mathbb{R}$,

$$\alpha_s \circ \alpha_t = \alpha_{s+t}.$$

This says that if we evolve a system from a time s and then evolve the system to a time t , this is the same as evolving the system directly to the time $s + t$.

To summarize the above explanations, mathematical models of physical systems have the following underlying framework:

1. A list of physical quantities that generate a C^* -algebra \mathcal{A} of *observables*.
2. *States* that are given by continuous linear functionals

$$\phi : \mathcal{A} \rightarrow \mathbb{C}$$

such that $\phi(1) = 1$ and has the properties that for all $a \in \mathcal{A}$,

$$\phi(a^*a) \geq 0 \text{ and } \phi(a^*) = \phi(a)^*.$$

3. A *time evolution* of the system given by a one-parameter group of automorphisms $\{\alpha_t \mid t \in \mathbb{R}\}$ on \mathcal{A} such that for times $s, t \in \mathbb{R}$,

$$\alpha_s \circ \alpha_t = \alpha_{s+t}.$$

Now that we have provided the framework for any physical model, let's focus on the differences between CM and QM models.

In a classical system, all operators commute with one another; the commutator between two elements a, b in an algebra of observables is zero,

$$[a, b] = ab - ba = 0.$$

The distinguishing characteristic of QM models is that operators do not all commute with one another. A common example of non-commuting observables in QM comes from the position operator \hat{x} and the momentum \hat{p}_x in the direction of x ,

$$[\hat{x}, \hat{p}_x] = \hat{x}\hat{p}_x - \hat{p}_x\hat{x} = i\hbar$$

where i is the imaginary unit and \hbar is Planck's constant. Classically, the commutator relation of position and momentum evaluates to zero.

We almost have all the ingredients necessary to quantize the ES model, but before we can get to writing down representations of operators that don't commute with one another, we need to define the space in which these operators reside. Namely, a Hilbert space where the unit vectors in this Hilbert space represent states.

3.2 A Hilbert Space for Observables

The Hilbert space \mathcal{H} we will be considering is the inner product space that is the complex span of the pruned tree \mathcal{T}_A denoted as $\text{span}_{\mathbb{C}}(\mathcal{T}_A)$ equip with the Euclidean inner product such that for all $a_k \in \mathcal{T}_A$,

$$\langle a_i | a_j \rangle = \delta_{ij}$$

where δ_{ij} is the Kronecker delta. Notionally, we denote such a Hilbert space as

$$\mathcal{H} := (\text{span}_{\mathbb{C}}(\mathcal{T}_A), \langle | \rangle).$$

Definition 3.1. A *pure state* $|a\rangle$ of a QM system is represented in a complex Hilbert space by a ray that is a set of nonzero vectors differing by normalized complex scalars. The inner product of $|a\rangle$ with itself is $\langle a | a \rangle = 1$.

Since \mathcal{H} is the complex span of \mathcal{T}_A , we can interpret pure states to be vectors $|v\rangle$ of linear combinations of A -admissible numbers $|a\rangle$

$$|v\rangle = \sum_{a \in \mathcal{T}_A} c_a |a\rangle \tag{39}$$

where $c_k \in \mathbb{C}$. An example of a unit pure state vector $|w\rangle$ is

$$|w\rangle = \frac{i}{\sqrt{2}} |a\rangle + \frac{-i}{\sqrt{2}} |b\rangle$$

where a, b must be A -admissible numbers. The inner product of $|w\rangle$ with itself is

$$\langle w | w \rangle = \left(\frac{i}{\sqrt{2}} \right)^2 + \left(\frac{-i}{\sqrt{2}} \right)^2 = 1.$$

We represent such an ensemble of pure states by a matrix called a density matrix.

Definition 3.2. A *density matrix* $\hat{\rho}$ of a QM system is the outer product of pure states $|a\rangle$,

$$\hat{\rho} = \sum_{a \in \mathcal{T}} p_a |a\rangle \langle a|$$

where a is a vertex in \mathcal{T} , $\hat{\rho}$ is a density matrix, $p_a \in (0, 1]$, and $\sum_{a \in \mathcal{T}_A} p_a = 1$.

State vectors correspond to density matrices by $p_a = |c_a|^2$ where c_a is as in (39).

3.3 Cuntz-Krieger Algebra

Now that we have defined a Hilbert space \mathcal{H} , we can define the operators of a C^* -algebra that reside in \mathcal{H} . The particular C^* -algebra we will be using to formulate a quantum mechanical model of ES is the *Cuntz-Krieger* (CK) algebra. This algebra was originally defined in [7] to provide a connection between C^* -algebras and Markov chains. Every Cuntz-Krieger algebra is associated with an incidence matrix that encodes the directions in which a system can transition and is the same incidence matrix seen in (33) when pruning the tree. A precise definition of the CK is provided below where $I \subset \mathbf{P} = \{0, 1, \dots, p-1\}$ and the cardinality of I is at least two.

Definition 3.3. Let A be an incidence matrix such that each row and column has at least one entry equal to one. The *Cuntz-Krieger algebra* \mathcal{O}_A associated with A is a C^* -algebra generated by non-zero partial isometries $\{S_i\}_{i \in I}$ of a complex Hilbert space satisfying the relations for all $i \in I$,

$$\sum_{j \in I} S_j S_j^* = 1 \quad \text{and} \quad S_i^* S_i = \sum_{j \in I} A_{ij} S_j S_j^*.$$

To see the noncommutative behavior of the Cuntz-Krieger (CK) algebra, let $\mathbf{P} = \{0, 1\}$ and consider the incidence matrix

$$A = \begin{pmatrix} 1 & 1 \\ 1 & 0 \end{pmatrix}$$

which corresponds to a CK-algebra \mathcal{O}_A . For $i = 0$,

$$S_0^* S_0 = \sum_j A_{0j} S_j S_j^* = A_{00} S_0 S_0^* + A_{01} S_1 S_1^*.$$

Since $A_{00} = 1$ and $A_{01} = 1$, then

$$S_0^* S_0 = S_0 S_0^* + S_1 S_1^*.$$

Thus, the commutator of S_0 and S_0^* for this particular incidence matrix A is

$$[S_0, S_0^*] = S_0 S_0^* - S_0^* S_0 = -S_1 S_1^* \neq 0.$$

Since there exists a pair of noncommuting elements in \mathcal{O}_A , this CK-algebra is noncommutative.

The only CK-algebra that has $S_i^* S_i = S_i S_i^*$ for all $i \in I$ is the CK-algebra associated with the incidence matrix the Kronecker delta δ_{ij} , in which case, this algebra is a Cuntz algebra [8].

3.4 Time Evolution in a Quantum Mechanical ES Model

The time evolution of a system can be specified by a single self-adjoint operator H known as the *Hamiltonian*. The Hamiltonian represents the possible outcomes when measuring the total energy of a system. The microscopic quantum mechanical nature of the system is described by the C^* -algebra of observables along with a time evolution given by a one-parameter family $\{\alpha_t \mid t \in \mathbb{R}\}$ of automorphisms depending on H .

Definition 3.4. *The **time evolution of a system** is an automorphism $\alpha_t : \mathcal{O}_A \rightarrow \mathcal{O}_A$ such that for all $j \in \mathbf{P}$,*

$$\alpha_t(S_j) = e^{itH} S_j$$

where H is the Hamiltonian of the system.

We will specialize this time evolution for the ES model to

$$\alpha_t(S_a) = q^{it} S_a \tag{40}$$

where $|\mathbf{P}| = q$.

3.5 States in a Quantum Mechanical ES Model

Now that we established a notion of time evolution, we look for equilibrium states that depend on the inverse temperature $\beta = (kT)^{-1}$ and for simplicity, set Boltzmann's constant $k \equiv 1$. In classical mechanics we consider the possible states a of the system that maintain equilibrium given by the Gibbs grand canonical equilibrium state,

$$\varphi(a) = \frac{1}{Z(\beta)} \text{Tr}(a e^{-\beta H})$$

where $Z(\beta)$ is the partition function given by $Z(\beta) = \text{Tr}(e^{-\beta H})$. A Gibbs equilibrium state is the state a system will end up in if allowed to thermalize, which is the process of physical bodies reaching thermal equilibrium through mutual interaction [8]. This means that Gibbs equilibrium states are those with the maximum entropy distribution for a given amount of energy in a system at time t .

If the Gibbs state at temperature t is known, then by taking a logarithm of $e^{-\beta H} = e^{-H/t}$ we can work out the Hamiltonian. This implies that specifying a Hamiltonian and specifying a Gibbs state are equivalent.

Notice that these Gibbs states are only well-defined only under the assumption that the operator $e^{-\beta H}$ is of trace class; the trace function can be defined for this operator. This becomes a problem when consider Hamiltonians of infinite systems, those with infinitely many particles, because these are not well-defined operators.

In the classical case, we can solve this problem by noticing that although the energy of an infinite configuration is undefined, the energy difference between two configurations differing only on a finite domain *is* well-defined. This leads to the the Dobrushin-Lanford-Ruelle (DLR) equation that characterizes equilibrium states in the classical setting.

In the quantum case, we take an alternative approach to solving this problem of an ill-defined Hamiltonian for infinite systems by generalizing our notion of an equilibrium state and considering the Kubo-Martin-Schwinger (KMS) condition [8].

Theorem 3.1. *Given a C^* -algebra \mathcal{A} with a one-parameter group of automorphisms, a state ϕ on \mathcal{A} satisfies the **KMS condition** at inverse temperature $\beta \in (0, \infty)$ if and only if for all $a, b \in \mathcal{A}$ there exists a bounded function $F_{a,b}(z)$ that is holomorphic on a continuous strip on length β and such that for all $t \in \mathbb{R}$,*

$$F_{a,b}(t) = \phi(a\alpha_t(b)) \quad \text{and} \quad F_{a,b}(t + i\beta) = \phi(\alpha_t(b)a).$$

Thus, the defining property of KMS state is their invariance under time evolution and thus depend of a notion of time with respect to the evolving system. This means that given a notion of time flow there is a notion of a KMS state.

The KMS states we are interested in the ES model are those with unique temperature that is equal to the Hausdorff dimension, $\beta = \delta_A = \log(\lambda_A)/\log(|\mathbf{P}|) = \dim(\partial\mathcal{T}_A)$. At this temperature, there is a unique KMS states given by

$$\phi(S_v S_w^*) = \begin{cases} \mu(\partial\mathcal{T}_A(a)) & v = w \in \mathcal{T}_A \\ 0 & v \neq w \in \mathcal{T}_A \end{cases}.$$

where $\mu(\partial\mathcal{T}_A(a))$ is defined in (35). Since the KMS states are dependent on time evolution, we look at our time evolution operator

$$\alpha_t = q^{it}$$

with $q = |\mathbf{P}|$ and notice that the self-similar measure $\mu(\partial\mathcal{T}_A)$ defined a KMS state at unique temperature δ_A , and versa vice since a unique temperature δ_A determines the KMS state.

4 Algebraic Structure of Anti-de Sitter Space

The goal of this section is to understand the analogy presented in *p-adic AdS/CFT* [14] between the Bruhat-Tits \mathcal{T}_n tree defined as the coset space

$$\mathcal{T}_2 := PGL(2, \mathbb{Q}_2)/PGL(2, \mathbb{Z}_2) \tag{41}$$

and Anti de Sitter (AdS) space defined as the coset space

$$AdS_2 := SO(2, 1)/SO(1, 1). \quad (42)$$

The Bruhat-Tits tree can be seen as a discrete analog of AdS and this analogy is used to formulate a p -adic AdS_2/CFT_1 correspondence.

Rather than jumping into calculating correlation functions in a p -adic version of AdS_2/CFT_1 , we separately examine the \mathcal{T}_2 and AdS_2 . Once we have constructed both in terms of coset spaces, then we examine the analogy between these spaces.

In this section, we present a new way of visualizing p -adic lattices and use these p -adic lattices to coordinatize the Bruhat-Tits tree. This new visualization of p -adic lattices is in contrast to previous work [4] where Zabrodin uses real lattices to define the Bruhat-Tits tree. In [14], the Bruhat-Tits tree is defined by using an unramified algebraic extension of \mathbb{Q}_p , but we do not make use of this definition.

4.1 Real Anti de Sitter Space

4.1.1 Generators of Flow

Let M be a (psuedo) Riemannian manifold with metric $g_{\mu\nu}$ and Levi-Civita connection ∇ . Let V be a smooth vector field on M . The vector field V generates a one-dimensional family of functions $f_V(t) : M \rightarrow M$ such that

$$f_V(\epsilon)(x) = x + \epsilon V + \mathcal{O}(\epsilon^2) \quad (43)$$

where t is a one-value parameter. Let T be a rank (m, n) -tensor on M ,

$$T_{\mu_1 \dots \mu_m}^{\nu_1 \dots \nu_n}. \quad (44)$$

The function f_V induces a function on tensors

$$f_V^*(\epsilon) T_{\mu_1 \dots \mu_m}^{\nu_1 \dots \nu_n}(x) = \underbrace{J \dots J}_{m \text{ times}} \underbrace{J^{-1} \dots J^{-1}}_{n \text{ times}} T_{\mu_1 \dots \mu_m}^{\nu_1 \dots \nu_n}(x + \epsilon V)$$

where J and J^{-1} are the Jacobian and inverse Jacobian, respectively,

$$J_{\mu}^{\nu} = \nabla_{\mu}(x^{\nu} + \epsilon V^{\nu}) = \delta_{\mu}^{\nu} + \epsilon \nabla_{\mu} V^{\nu}$$

and

$$(J_{\nu}^{\mu})^{-1} = \nabla_{\mu}(x^{\nu} - \epsilon V^{\nu}) = \delta_{\mu}^{\nu} - \epsilon \nabla_{\mu} V^{\nu}.$$

Expanding $T(x + \epsilon V) = T(x) + \epsilon \nabla T(x) + \mathcal{O}(\epsilon^2)$ and distributing. Then

$$f_V^*(\epsilon) T(x) = T(x) + \epsilon \left(\nabla T - \underbrace{T \nabla V}_{m \text{ times}} + \underbrace{T \nabla V}_{n \text{ times}} \right) + \mathcal{O}(\epsilon^2)$$

where $\nabla T - \underbrace{T \nabla V}_{m \text{ times}} + \underbrace{T \nabla V}_{n \text{ times}}$ is the generator of flows along V . The vector field V generates isometries if $\mathcal{L}_V T = 0$. The vector field V generators flows for points on a manifold and the Lie derivative \mathcal{L}_V generators flows for tensors. We discuss the Lie derivative in the next section.

4.1.2 Lie Derivatives and the Killing Equation

The *Lie derivative* \mathcal{L}_V is a derivative of a tensor field along a vector field V . When applied to vector fields and one-forms, the Lie derivative acts as

$$\mathcal{L}_V X^\mu = V^\nu \partial_\nu X^\mu - (\partial_\nu V^\mu) X^\nu \quad (45)$$

and

$$\mathcal{L}_V Y_\mu = V^\nu \partial_\nu Y_\mu - (\partial_\mu V^\nu) Y_\nu \quad (46)$$

respectively. If we have the Levi-Civita connection, then the partial derivatives ∂_μ above can be replaced by covariant derivatives ∇_μ . It's useful to know how \mathcal{L}_V acts on symmetric forms since spacetime metrics $g_{\mu\nu}$ are among these. If we have a torsion-free connection, $\nabla_\rho g_{\mu\nu} = 0$, then the \mathcal{L}_V acts on metrics as

$$\mathcal{L}_V g_{\mu\nu} = V^\rho \nabla_\rho g_{\mu\nu} + (\nabla_\mu V^\rho) g_{\rho\nu} + (\nabla_\nu V^\rho) g_{\mu\rho} = \nabla_\mu V_\nu + \nabla_\nu V_\mu = 2\nabla_{(\mu} V_{\nu)}. \quad (47)$$

The equation

$$\nabla_\mu V_\nu + \nabla_\nu V_\mu = 0 \quad (48)$$

is known as the *Killing equation*. Vector fields V^μ that satisfy the Killing equation are those that leave the metric invariant are known as *Killing vector fields*, i.e.

$$\mathcal{L}_V g_{\mu\nu} = 0 \quad (49)$$

if and only if the flows of V are isometries, so $f_V^* : M \rightarrow M$ such that

$$f_V^* g = g. \quad (50)$$

where $g_{\mu\nu}$ is a spacetime metric.

4.1.3 Maximally Symmetric Spaces

Since AdS is a maximally symmetric space, we are going to discuss such spaces in detail.

The symmetries of spacetime are given by Killing vector fields X which by definition satisfy

$$\mathcal{L}_X g_{\mu\nu} = 0 \quad (51)$$

where $g_{\mu\nu}$ is a spacetime metric. A Killing vector field is linearly dependent if it can be written as a linear combination of other Killing vector fields with constant coefficients.

The question now becomes, how many linearly independent Killing vector fields can a space have? In other words, how many independent one-dimensional families of isometries can a manifold have? Since all manifolds are locally Euclidean, i.e. around every point, there is a neighborhood that is topologically the same as the open unit ball in \mathbb{R}^n , then let's examine the isometries of the space \mathbb{R}^n . These are translations and rotations in n -dimensions. The translations are transformations that move a point on a manifold, so there are n independent axes along which a point can be moved. This means there are n total translations. Rotations, centered at p on a manifold, are the transformations that leave p

invariant after moving one of the axes through p into another axis. There are n axes to choose from and $n - 1$ other axes that can be rotated into. Since we don't treat a rotation from x into y and a rotation from y into x as different, there are $\binom{n}{2} = \frac{1}{2}n(n - 1)$ rotations. Therefore, there are

$$n + \frac{1}{2}n(n - 1) = \frac{1}{2}n(n + 1) \quad (52)$$

independent symmetries of \mathbb{R}^n .

This combinatorial argument only refers to the behavior of the symmetry in a neighborhood at a point, but not globally on the manifold. In the presence of curvature, this local counting argument should be the same. When the metric is not Euclidean, say Lorentzian, some of the rotations will be boost transformations. But this counting argument remains the same. But let's explicitly check this by examining Minkowski space.

Example 4.1. Consider the flat spacetime with the Minkowski metric $\eta_{\mu\nu}$ with signature $(-, +, +, +)$. In Cartesian coordinates $(x^0, x^1, x^2, x^3) = (t, x, y, z)$, the metric is

$$\eta_{\mu\nu} = \begin{pmatrix} -1 & & & \\ & 1 & & \\ & & 1 & \\ & & & 1 \end{pmatrix}$$

and the Christoffel connection vanishes. Thus, we can replace the covariant derivative by partial derivatives, and the Killing equation (48) becomes

$$\partial_\beta X_\alpha + \partial_\alpha X_\beta = 0. \quad (53)$$

Taking a second derivative gives

$$\partial_\gamma \partial_\beta X_\alpha + \partial_\gamma \partial_\alpha X_\beta = 0.$$

Then cycling the indices gives

$$\begin{aligned} \partial_\gamma \partial_\beta X_\alpha + \partial_\gamma \partial_\alpha X_\beta &= 0, \\ \partial_\gamma \partial_\alpha X_\alpha + \partial_\alpha \partial_\beta X_\gamma &= 0, \\ \partial_\beta \partial_\alpha X_\alpha + \partial_\beta \partial_\gamma X_\alpha &= 0. \end{aligned}$$

Adding the first two and subtracting the third results in

$$0 = \partial_\beta \partial_\gamma X_\alpha + \partial_\alpha \partial_\gamma X_\beta + \partial_\gamma \partial_\alpha X_\beta + \partial_\beta \partial_\alpha X_\gamma - \partial_\alpha \partial_\beta X_\gamma - \partial_\gamma \partial_\beta X_\alpha = 2\partial_\alpha \partial_\gamma X_\beta.$$

Thus, second derivatives of X_β vanish. This means that X_β must be linear in the coordinates

$$X_\alpha = v_\alpha + w_{\alpha\beta} x^\beta. \quad (54)$$

Substituting this into the Killing equation yields

$$0 = \partial_\beta X_\alpha + \partial_\alpha X_\beta = w_{\alpha\beta} + w_{\beta\alpha}$$

which implies that v_α is arbitrary while $w_{\alpha\beta}$ must be antisymmetric.

All of the isometries we can find will be of the form

$$X_\alpha = v_\alpha + w_{\alpha\beta}x^\beta$$

for independent choices of constants. Let's take $w_{\alpha\beta} = 0$ and one of the components, the n th component, of v_α to be nonzero. Then we get four constant vector fields

$$X_{(n)}^\alpha = \delta_n^\alpha.$$

This represents a unit vector in each of the coordinate directions. Thus, we have 4 translations.

Now setting $v_\alpha = 0$ and choosing one of six antisymmetric matrices $w_{\alpha\beta}$, we have either rotations or boosts. For example, with $w_{21} = -w_{12} = 1$ with all other entries equal to zero. Then the vector field is

$$X = X^\alpha \partial_\alpha = (\eta^{\alpha\beta} w_{\beta\gamma} x^\gamma) \partial_\alpha = x \frac{\partial}{\partial y} - y \frac{\partial}{\partial x}.$$

This is the generator of a rotation around the z axis. This can be repeated with $w_{23} = -w_{32} = 1$ and $w_{31} = -w_{13} = 1$ to obtain the generators of rotations around the x and y axes. Now if we take one of the nonzero indices to be time, say $b_{10} = -b_{01} = 1$, then we have

$$X = X^\alpha \partial_\alpha = (\eta^{\alpha\beta} w_{\beta\gamma} x^\gamma) \partial_\alpha = x \frac{\partial}{\partial t} + t \frac{\partial}{\partial x}.$$

This is a generator for a Lorentz boost in the x direction. This can be repeated with $w_{02} = -w_{20} = 1$ and $w_{03} = -w_{30} = 1$ to obtain the Lorentz boosts in the y and z directions.

We have exhausted the possibilities for the possible linear independent vectors fields $X_\alpha = v_\alpha + w_{\alpha\beta}x^\beta$ and have found exactly 10 isometries (4 translations, 3 rotations, 3 boosts) in Minkowski space. This is one instance of verifying the claim that there are $n(n+1)/2$ isometries for Minkowski space. Thus, Minkowski space is maximally symmetric.

For a maximally symmetric spacetime, the curvature must be the same everywhere. We are able to express the Riemann $R_{\mu\nu\rho\sigma}$ curvature tensor in terms of the Ricci scalar R . Using the symmetries of $R_{\mu\nu\rho\sigma}$, we have

$$R_{\mu\nu\rho\sigma} = \frac{R}{(n-1)(n-2)} (g_{\nu\sigma}g_{\mu\rho} - g_{\nu\rho}g_{\mu\sigma}). \quad (55)$$

Therefore, we can classify maximally symmetric spacetimes according to their dimensions, the value of the Ricci scalar, and the signature of the spacetime metric. This means that the only possible types of curvature a maximally symmetric space can have is positive, negative, or zero curvature.

If we consider the case of Riemannian manifolds, the maximally symmetric spacetimes are globally Euclidean, spherical, or hyperbolic. The line element of these spaces can be written as

$$ds^2 = \frac{d\chi^2}{1 - k\chi^2} + \chi^2 d\Omega_{n-1}^2 \equiv dK_n^2 \quad (56)$$

where $k \in \{0, \pm 1\}$ and $d\Omega_{d-1}^2$ is the line elements of a unit sphere S^{n-1} . We can iteratively define $d\Omega_{n-1}^2$ by

$$d\Omega_1 = d\theta_1, \quad d\Omega_j^2 = d\theta_j^2 + \sin^2 \theta_j d\Omega_{j-1}^2 \quad (57)$$

where $\theta_1 \in [0, 2\pi)$ and $\theta_j \in [0, \pi)$ for $j \in \{2, \dots, n-2\}$.

If we consider the case of Lorentzian manifolds, then we find three maximally symmetric spacetimes that depend on the sign of the Ricci scalar R . For $R = 0$, the maximally symmetric spacetime is Minkowski. For $R > 0$, the maximally symmetric spacetime is known as de Sitter spacetime. For $R < 0$, the maximally symmetric spacetime is Anti de Sitter spacetime.

4.1.4 Anti de Sitter Spacetime

Anti de Sitter (AdS) spacetime is a n -dimensional maximally symmetric spacetime with negative constant scalar curvature.

The n -dimensional Anti de Sitter space, AdS_n , can be embedded into $n+1$ -dimensional twotime space with coordinate $(x^0, x^1, \dots, x^n) \in \mathbb{R}^{n-1,2}$ with the metric

$$ds^2 = -(dx^0)^2 + (dx^1)^2 + \dots + (dx^{n-1})^2 - (dx^n)^2 \equiv g_{\mu\nu} dx^\mu dx^\nu \quad (58)$$

where $\mu, \nu \in \{0, 1, \dots, n\}$. Note the signature of the metric, $g = \text{diag}(-, +, \dots, +, -)$, which has two negative time entries.

In particular, AdS_n is given by the hypersurface

$$g_{\mu\nu} x^\mu x^\nu = -(x^0)^2 + \sum_{i=1}^{n-1} (x^i)^2 - (x^n)^2 = -R^2 \quad (59)$$

embedded in $\mathbb{R}^{n-1,2}$. The value R corresponds to the radius of curvature in AdS. The hypersurface given by (59) is invariant under $O(n-1, 2)$ transformations acting on $\mathbb{R}^{n-1,2}$ which means that the isometry group of AdS_n contains $O(n-1, 2)$. Just as n -dimensional Minkowski space has $n(n+1)/2$ Killing vector fields, the group $O(n-1, 2)$ has $n(n+1)/2$ generators where every generator specifies a Killing vector. This implies that Anti de Sitter space is also maximally symmetric.

Let's study AdS_n is the following coordinate system. Let

$$\begin{aligned} X^0 &= R \cosh \rho \cos \tau, \\ X^n &= R \cosh \rho \sin \tau, \\ X^i &= R \Omega_i \sinh \rho \end{aligned}$$

for $i = 1, \dots, n-1$, and where Ω_i are angular coordinates satisfying $\sum_i \Omega_i^2 = 1$. In other words, Ω_i parametrizes a $(n-1)$ -dimensional sphere S^{n-1} . The remaining coordinates take the ranges $\rho \in \mathbb{R}_+$ and $\tau \in [0, 2\pi)$. We refer to (ρ, τ, Ω_i) as global coordinates on AdS_n since all points of the hypersurface are taken into account exactly once.

Let's examine AdS_2 spacetime embedded into $\mathbb{R}^{1,2}$. The global coordinates are

$$\begin{aligned} X^0 &= R \cosh \rho \cos \tau, \\ X^1 &= R \Omega_1 \sinh \rho, \\ X^2 &= R \cosh \rho \sin \tau. \end{aligned} \quad (60)$$

Inserting (60) into (58) yields the metric

$$ds^2 = R^2(-\cosh^2 \rho d\tau^2 + d\rho^2 + \sinh^2 \rho d\Omega_{n-2}^2). \quad (61)$$

4.1.5 Transitive $SO(1,2)$ action on AdS_2

In the previous section we established AdS_2 as the solution set,

$$\text{AdS}_2 := \{(x_0, x_1, x_2) \in \mathbb{R}^3 \mid -x_0^2 + x_1^2 - x_2^2 = -R^2\}. \quad (62)$$

This solution set is a hyperboloid of one sheet in $\mathbb{R}^{2,1}$.

Definition 4.1. A group G acts **transitively** on a space X if for any two distinct points $p, q \in X$, there exists $g \in G$, such that $g(p) = q$.

Theorem 4.1. $SO(1,2)$ acts transitively on AdS_2 .

Proof. We need to show that for all $\vec{x} = (x_0, x_1, x_2)$ and $\vec{y} = (y_0, y_1, y_2)$ in AdS_2 , there exists a matrix $M \in SO(1,2)$ such that

$$M\vec{x} = \vec{y}. \quad (63)$$

Rotating the x_0 axis into the x_2 axis by a rotation matrix $M_1 \in SO(1,2)$ to $\vec{x} = (x_0, x_1, x_2)$ yields

$$\begin{pmatrix} \frac{x_0}{\sqrt{x_0^2+x_2^2}} & 0 & \frac{x_2}{\sqrt{x_0^2+x_2^2}} \\ 0 & 1 & 0 \\ -\frac{x_2}{\sqrt{x_0^2+x_2^2}} & 0 & \frac{x_0}{\sqrt{x_0^2+x_2^2}} \end{pmatrix} \begin{pmatrix} x_0 \\ x_1 \\ x_2 \end{pmatrix} = \begin{pmatrix} \frac{x_0^2+x_2^2}{\sqrt{x_0^2+x_2^2}} \\ x_1 \\ 0 \end{pmatrix} = \begin{pmatrix} \sqrt{x_0^2+x_2^2} \\ x_1 \\ 0 \end{pmatrix}. \quad (64)$$

Let $R := \sqrt{x_0^2+x_2^2}$ and $\gamma = 1/\sqrt{x_1^2-R^2}$, then applying a Lorentz boost matrix M_2 in the x_1 -direction yields

$$\begin{pmatrix} \gamma R & -\gamma x_1 & 0 \\ -\gamma x_1 & \gamma R & 0 \\ 0 & 0 & 1 \end{pmatrix} \begin{pmatrix} R \\ x_1 \\ 0 \end{pmatrix} = \begin{pmatrix} \gamma(R^2-x_1^2) \\ \gamma(Rx_1-Rx_1) \\ 0 \end{pmatrix} = \begin{pmatrix} -\sqrt{R^2-x_1^2} \\ 0 \\ 0 \end{pmatrix} = \begin{pmatrix} -\sqrt{-x_0^2+x_1^2-x_2^2} \\ 0 \\ 0 \end{pmatrix}. \quad (65)$$

So we have

$$M_2 M_1 \vec{x} = R \begin{pmatrix} 1 \\ 0 \\ 0 \end{pmatrix}. \quad (66)$$

Since every point in AdS_2 is a linear combination of basis vectors $\left\{ \begin{pmatrix} 1 \\ 0 \\ 0 \end{pmatrix}, \begin{pmatrix} 0 \\ 1 \\ 0 \end{pmatrix}, \begin{pmatrix} 0 \\ 0 \\ 1 \end{pmatrix} \right\}$, we can repeat a similar computation to go from \vec{x} to \vec{y} . Such transformations will always involve a rotation and a Lorentz boost. \square

4.1.6 Constructing AdS_2 as a Coset Space

It is useful to view a maximally symmetric spacetime as a *coset space*. Such a space is obtained by modding out the isometry group of the spacetime by the stabilizer group for a point on the spacetime. The stabilizer group contains those isometries which leave a point invariant.

Theorem 4.2. *Let a group G act transitively on a set X . Then there is a isomorphism between X and the quotient group $G/\text{stab}_G(x_0)$ for any $x_0 \in X$, given by $f : G/\text{stab}_G(x_0) \rightarrow X$ such that*

$$g \cdot \text{stab}_G(x_0) \mapsto g \cdot x_0 \quad (67)$$

where $g \in G$.

Example 4.2. *Consider the 2-sphere S^2 . The isometry group is $SO(3)$. Each point p on S^2 is invariant under the rotations around the axis connecting the center of the sphere to p . Then by Theorem 4.2, S^2 is given by the coset space $SO(3)/SO(2)$. We can generalize this to n -dimensions where S^n corresponds to $SO(n+1)/SO(n)$.*

Using Theorem 4.2 and Theorem 4.1, we define AdS_2 as the coset space

$$\text{AdS}_2 := SO(1,2)/SO(1,1). \quad (68)$$

4.2 p-adic Anti de Sitter Space

The definition of the Bruhat-Tits tree that we are interested in is one that involves \mathbb{Z}_p -lattices. The next several sections discuss such lattices.

4.2.1 \mathbb{Z} -lattices in \mathbb{R}^2 versus \mathbb{Z}_p -lattices in \mathbb{Q}_p^2 .

Definition 4.2. *A lattice \mathcal{L} in \mathbb{R}^2 is a rank two \mathbb{Z} -submodule of \mathbb{R}^2 .*

In other words, if there exists two linearly independent vectors $v_1, v_2 \in \mathbb{R}^2$ such that

$$\mathcal{L} = \{av_1 + bv_2 \mid a, b \in \mathbb{Z}\},$$

then \mathcal{L} is a lattice in \mathbb{R}^2 . Two lattices \mathcal{L}_1 and \mathcal{L}_2 are equivalent if for some nonzero $\lambda \in \mathbb{R}^*$,

$$\mathcal{L}_1 = \lambda\mathcal{L}_2$$

or for some rotation matrix R . We can define \mathbb{Z}_p -lattices in \mathbb{Q}_p in a very similar way by replacing \mathbb{R}^2 with \mathbb{Q}_p^2 and \mathbb{Z} with \mathbb{Z}_p .

Definition 4.3. *A lattice \mathcal{L} in \mathbb{Q}_p^2 is a rank two \mathbb{Z}_p -submodule of \mathbb{Q}_p^2 .*

So if there exists two linearly independent vectors $v_1, v_2 \in \mathbb{Q}_p^2$ such that

$$\mathcal{L} = \{av_1 + bv_2 \mid a, b \in \mathbb{Z}_p\},$$

then \mathcal{L} is a lattice in \mathbb{Q}_p^2 . Two lattices \mathcal{L}_1 and \mathcal{L}_2 are equivalent if for some nonzero $\lambda \in \mathbb{Q}_p^*$,

$$\mathcal{L}_1 = \lambda \mathcal{L}_2.$$

We are now posed with a problem since it is not immediately obvious how to visualize such a \mathbb{Z}_p -lattice.

Additionally, for \mathbb{Z} -lattices, we're able to visualize them in \mathbb{R}^2 because we have a way of drawing \mathbb{R}

Additionally, for \mathbb{Z} -lattices, we're able to visualize them in \mathbb{R}^2 because we have and make use of the parallelogram law when adding vectors together. However, there is no standard way of drawing \mathbb{Q}_p^2 and since \mathbb{Q}_p has a non-Archimedean norm, we can't make use of the parallelogram law.

In the following sections we present a way to visualize \mathbb{Q}_p^2 , along with a new visualization for \mathbb{Z}_p -lattices in \mathbb{Q}_p^2 .

4.2.2 Visualizing \mathbb{Q}_p and \mathbb{Q}_p^2

Just as we visualize elements in the real numbers \mathbb{R} as points on the real number line, we would like to be able to identify elements in \mathbb{Q}_p as points on a \mathbb{Q}_p number line. To do this, we need to first construct the \mathbb{Q}_p number line.

Every p -adic number x has a power series representation,

$$x = \sum_{n=m}^{\infty} a_n p^n \quad (69)$$

for $x_n = 0, \dots, p-1$ and m is the p -adic valuation. This means that all $x \in \mathbb{Q}_p$ are combinations of elements from $\{0, 1, \dots, p-1\}$. For example, elements of \mathbb{Q}_3 are built out of combinations of elements in $\{0, 1, 2\}$. The number 25 in base 10 is $\bar{0}221.0$ in \mathbb{Q}_3 since

$$\sum_{n=\min}^{\infty} a_n 3^n = 1 \cdot 3^0 + 2 \cdot 3^1 + 2 \cdot 3^2 + 0 \cdot 3^3 + 0 \cdot 3^4 + \dots = 25 \quad (70)$$

We identify $a_0 = 1$, $a_1 = 2$, $a_2 = 2$, $a_{m_i} = 0$ where $m \geq 3$ and $i = 1, 2, \dots$, then write this as

$$a_{m_i} a_2 a_1 a_0 . 0 = \bar{0}221.0 \quad (71)$$

This motivates the construction of the \mathbb{Q}_p number line is as follows. Draw a line segment ℓ and partition ℓ into $p-1$ equally spaced pieces. Label each partition mark with $\{0, 1, \dots, p-1\}$ using the usual ordering of the integers. Then in each subinterval, make another $p-1$ partitions. Since there are infinitely many subintervals, we stop partitioning after an adequate number of partitions.

As an example, consider the 2-adic integer number line \mathbb{Z}_2 ,

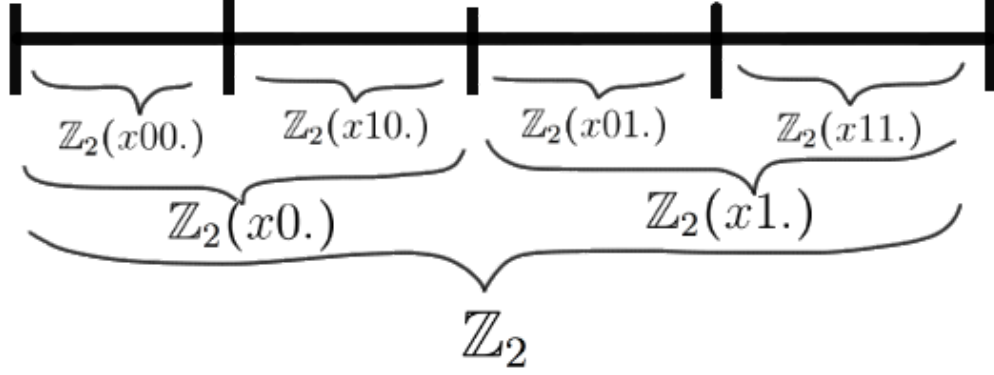


Figure 4: \mathbb{Z}_2 number line

where the intervals are defined as follows:

$$\begin{aligned}
 \mathbb{Z}_2(x0.) &= \{x0. \mid x \in \mathbb{Z}_2\}, \\
 \mathbb{Z}_2(x1.) &= \{x1. \mid x \in \mathbb{Z}_2\}, \\
 \mathbb{Z}_2(x00.) &= \{x00. \mid x \in \mathbb{Z}_2\}, \\
 \mathbb{Z}_2(x10.) &= \{x10. \mid x \in \mathbb{Z}_2\}, \\
 \mathbb{Z}_2(x01.) &= \{x01. \mid x \in \mathbb{Z}_2\}, \\
 \mathbb{Z}_2(x11.) &= \{x11. \mid x \in \mathbb{Z}_2\}.
 \end{aligned}$$

All intervals of the \mathbb{Z}_2 number line are of the form

$$\mathbb{Z}_2(xa_i.) = \{ax. \mid x \in \mathbb{Z}_2, a_i \in \{0, 1\}\}. \quad (72)$$

where a_i is finite. This generalizes to all subintervals of \mathbb{Z}_p being of the form

$$\mathbb{Z}_p(xa_i.) = \{ax. \mid x \in \mathbb{Z}_p, a_i \in \{0, 1, \dots, p-1\}\} \quad (73)$$

where a_i is finite.

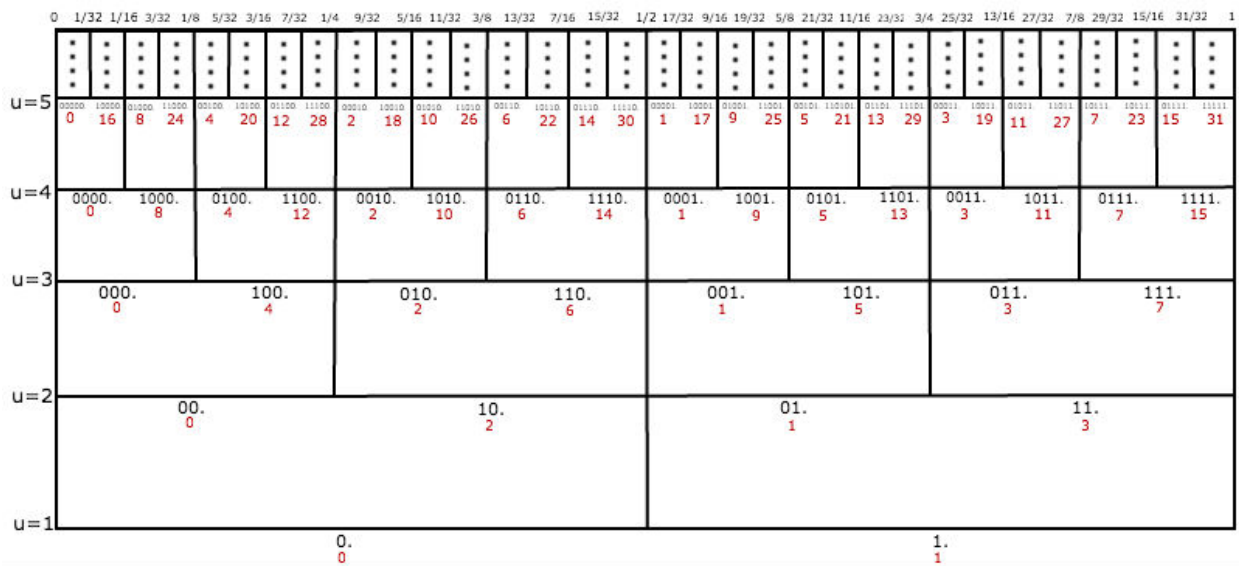
Let's continue to specialize to $p = 2$ and plot the element $\bar{0}10110.0 \in \mathbb{Q}_2$, which is 22 in base 10, on the \mathbb{Q}_2 number line. To do this, we choose subintervals in steps:

1. There is a 0 in the 2^0 position, so we choose the subinterval $\mathbb{Z}_2(x0.)$.
2. There is a 1 in the 2^1 position, so we choose the subinterval $\mathbb{Z}_2(x10.)$.
3. There is a 1 in the 2^2 position, so we choose the subinterval $\mathbb{Z}_2(x110.)$.
4. There is a 0 in the 2^3 position, so we choose the subinterval $\mathbb{Z}_2(x0110.)$.
5. There is a 1 in the 2^4 position, so we choose the subinterval $\mathbb{Z}_2(x10110.)$.
6. There is a recurring 0 for 2^m where $m > 4$, so we continue to choose subintervals of the form

$$\mathbb{Z}_2(\dots 00010110.)$$

and plot the point $\bar{0}10110.0$ where these subintervals converge.

We draw the position on the \mathbb{Q}_2 number line by placing a point on the endpoint of the subinterval $\mathbb{Z}_2(x10110.)$. We introduce the following chart. The index u labels each horizontal



level and increases from the bottom to the top of the chart. This chart only displays the first $2^5 - 1$ integers. Note that on each level u , there are the first $2^u - 1$ integers displayed. Each finite base 2 number is written in black with its equivalent expression as a base 10 number in red. The order in which these base 10 integers appear² from left to right on each level will become important when plotting p -adic integer lattices in the next section. Because of this importance, we note that the first few sequences of numbers appear as

$$\mathbf{u=1} \quad 0 \ 1, \tag{74}$$

$$\mathbf{u=2} \quad 0 \ 2 \ 1 \ 3, \tag{75}$$

$$\mathbf{u=3} \quad 0 \ 4 \ 2 \ 6 \ 1 \ 5 \ 3 \ 7 \tag{76}$$

Reading off this chart, we see that $\bar{0}10.0$ converges at $1/4$, $\bar{0}1001.$ converges at $9/16$, and $\bar{0}11110.0$ converges at $15/32$. It is useful to note that all numbers that are even in base 10 lie in the subinterval $[0, 1/2)$ and all numbers that are odd in base 10 lie in the subinterval $[1/2, 1)$.

An important thing to realize here is that there is nothing special about the real number coordinates placed at the top of this chart. We chose the interval $[0, 1]$ and then partitioned it into 32 subintervals, but we could have chosen the interval $[3, 234]$ and partitioned it into 32 subintervals. It is the number of partitions that is important here, not the real number coordinates.

Now let's take two copies of \mathbb{Z}_2 and draw \mathbb{Z}_2^2 as we would typically draw the first quadrant of the \mathbb{R}^2 plane. To distinguish between axes, we label $\mathbb{Z}_{2,x}$ and $\mathbb{Z}_{2,y}$ on the diagram (ref) and define ordered pairs as (x, y) where $x \in \mathbb{Z}_{2,x}$ and $y \in \mathbb{Z}_{2,y}$. Using the procedure from above,

²This is sequence A030109 on OEIS

we can plot points in \mathbb{Z}_2^2 . As an example, let's plot $(\bar{0}\bar{1}10.0, \bar{1}.0)$ in \mathbb{Z}_2^2 which is depicted in 5.

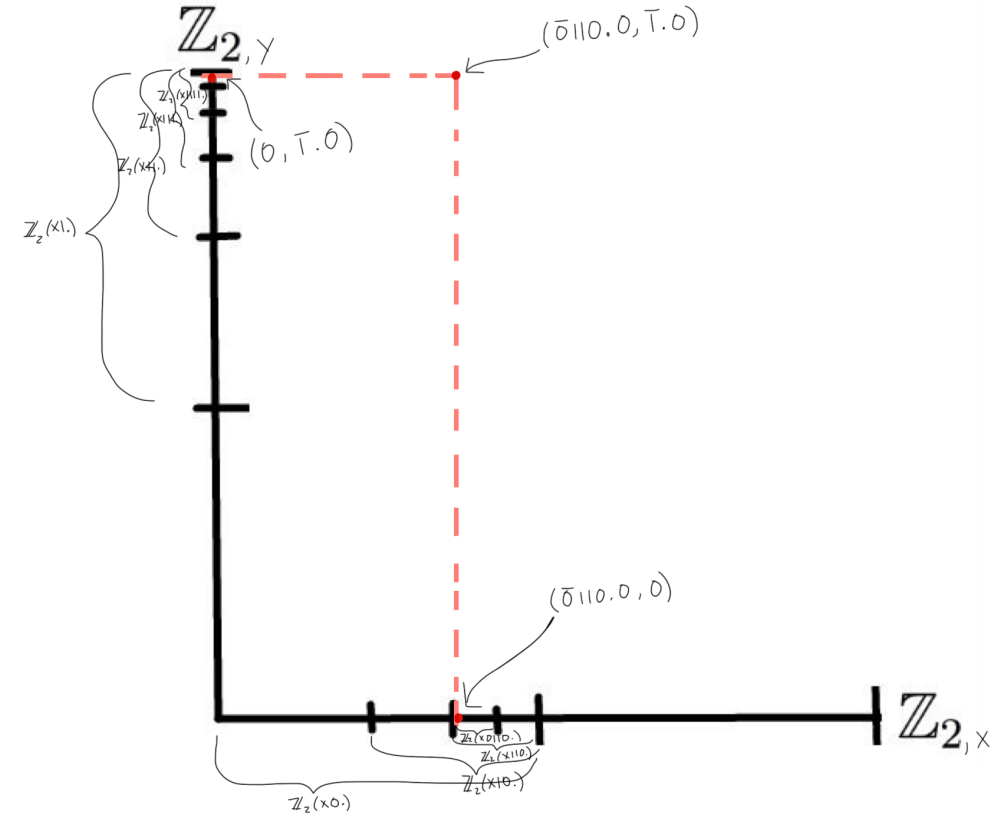


Figure 5: Plotting the point $(\bar{0}\bar{1}10.0, \bar{1}.0)$ in \mathbb{Z}_2^2 .

4.2.3 Visualizing p -adic Integer Lattices

The goal of this section is to use the method of plotting points in \mathbb{Z}_2^2 discussed in the previous section to plot the span of p -adic vectors and visualize p -adic integer lattices. For the remainder of the paper, we will specialize to $p = 2$ unless otherwise stated.

Definition: A \mathbb{Z}_2 -lattice in \mathbb{Q}_2^2 is the span of two linearly independent vector $v_1, v_2 \in \mathbb{Q}_2^2$ such that

$$\mathcal{L} := \text{span}_{\mathbb{Z}_2}\{v_1, v_2\} = \{av_1 + bv_2 \mid a, b \in \mathbb{Z}_2, v_1, v_2 \in \mathbb{Z}_2^2\}.$$

Plotting individual points in \mathbb{Q}_2^2 to make up the span of these vectors would take a very long time. So let's develop a method for quickly determining the $\text{span}_{\mathbb{Z}_2}\{v_1, v_2\}$. To do this, we work out an example.

Example 1. Consider the two linearly independent vectors

$$v_1 = (\bar{0}\bar{1}00.0, 0)_2 = (2^2, 0)_{10}$$

and

$$v_2 = (\overline{01.0}, \overline{01.0})_2 = (1, 1)_{10}$$

where the subscripts on these vectors denote which base the vector components are written in. For instance, $(\cdot, \cdot)_2$ means that the vector components are written in base 2, while $(\cdot, \cdot)_{10}$ means the vector components are written in base 10. The reason we occasionally convert from base 2 to base 10 is because it is usually easier to perform arithmetic in base 10.

To goal is to plot

$$\text{span}_{\mathbb{Z}_2} \left\{ \begin{pmatrix} 2^2 \\ 0 \end{pmatrix}, \begin{pmatrix} 1 \\ 1 \end{pmatrix} \right\} = \left\{ \alpha \begin{pmatrix} 2^2 \\ 0 \end{pmatrix} + \beta \begin{pmatrix} 1 \\ 1 \end{pmatrix} \mid \alpha, \beta \in \mathbb{Z}_2 \right\}. \quad (77)$$

Let's allow $\alpha \in \mathbb{Z}_2$ to vary in value and fix β to be $(2^2n + 0)$, $(2^2n + 1)$, $(2^2n + 2)$, $(2^2n + 3)$ where $n \in \mathbb{Z}_2$:

$$\begin{aligned} \text{(0)} \quad & \alpha \begin{pmatrix} 2^2 \\ 0 \end{pmatrix} + (2^2n + 0) \begin{pmatrix} 1 \\ 1 \end{pmatrix} = \begin{pmatrix} 4(\alpha+n)+0 \\ 4n+0 \end{pmatrix}, \\ \text{(1)} \quad & \alpha \begin{pmatrix} 2^2 \\ 0 \end{pmatrix} + (2^2n + 1) \begin{pmatrix} 1 \\ 1 \end{pmatrix} = \begin{pmatrix} 4(\alpha+n)+1 \\ 4n+1 \end{pmatrix}, \\ \text{(2)} \quad & \alpha \begin{pmatrix} 2^2 \\ 0 \end{pmatrix} + (2^2n + 2) \begin{pmatrix} 1 \\ 1 \end{pmatrix} = \begin{pmatrix} 4(\alpha+n)+2 \\ 4n+2 \end{pmatrix}, \\ \text{(3)} \quad & \alpha \begin{pmatrix} 2^2 \\ 0 \end{pmatrix} + (2^2n + 3) \begin{pmatrix} 1 \\ 1 \end{pmatrix} = \begin{pmatrix} 4(\alpha+n)+3 \\ 4n+3 \end{pmatrix}. \end{aligned}$$

The set of points of the form $\begin{pmatrix} 4(\alpha+n)+0 \\ 4n+0 \end{pmatrix}$ lie in $\mathbb{Z}_2(x00.) \times \mathbb{Z}_2(x00.)$. Similarly, the set of points of the form $\begin{pmatrix} 4(\alpha+n)+1 \\ 4n+1 \end{pmatrix}$ lie in $\mathbb{Z}_2(x10.) \times \mathbb{Z}_2(x10.)$. We visualize this 2-adic lattice in Fig. 6.

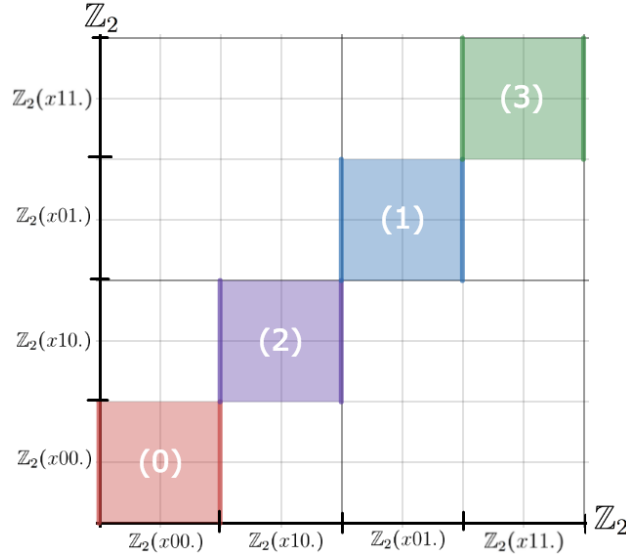


Figure 6: $\text{span}_{\mathbb{Z}_2} \left\{ \begin{pmatrix} 2^2 \\ 0 \end{pmatrix}, \begin{pmatrix} 1 \\ 1 \end{pmatrix} \right\}$

We can see that these rectangles were placed in the same order as (75). We will use this ordering to redefine out subintervals.

$$0 \times 0 := \mathbb{Z}_2(x00.) \times \mathbb{Z}_2(x00.), \quad (78)$$

$$1 \times 1 := \mathbb{Z}_2(x10.) \times \mathbb{Z}_2(x10.), \quad (79)$$

$$2 \times 2 := \mathbb{Z}_2(x01.) \times \mathbb{Z}_2(x01.), \quad (80)$$

$$3 \times 3 := \mathbb{Z}_2(x11.) \times \mathbb{Z}_2(x11.). \quad (81)$$

Similarly, when we write 1×2 and 3×0 , we refer to the rectangular regions

$$\begin{aligned} 1 \times 2 &:= \mathbb{Z}_2(x01) \times \mathbb{Z}_2(x10), \\ 3 \times 0 &:= \mathbb{Z}_2(x11.) \times \mathbb{Z}_2(x00.). \end{aligned}$$

Using this new identification of subintervals, we can quickly plot spans by looking at the least non-negative residue in each of the vector components. For instance, $\binom{4(\alpha+n)+0}{4n+0}$ has least nonnegative residue of 0 in the first component and least nonnegative residue of 0 in the second component. This means that $\binom{4(\alpha+n)+0}{4n+0}$ is the rectangular region 0×0 . Similarly, $\binom{4(\alpha+n)+1}{4n+1}$ is the rectangular region 1×1 .

Let's work on another example to become more familiar with the process of drawing spans of p -adic vectors.

Example 2 Consider the linearly independent vectors

$$v_1 = (\bar{0}100.0, 0)_2 = (2^2, 0)_{10}$$

and

$$v_2 = (\bar{0}10.0, \bar{0}1.0)_2 = (2, 1)_{10}.$$

We want to plot

$$\text{span}_{\mathbb{Z}_2} \left\{ \binom{2^2}{0}, \binom{2}{1} \right\} = \left\{ \alpha \binom{2^2}{0} + \beta \binom{2}{1} \mid \alpha, \beta \in \mathbb{Z}_2 \right\}. \quad (82)$$

Let's allow $\alpha \in \mathbb{Z}_2$ to vary in value and fix β to be (2^2n+0) , (2^2n+1) , (2^2n+2) , (2^2n+3) where $n \in \mathbb{Z}_2$:

$$\begin{aligned} \text{(0)} \quad & \alpha \binom{2^2}{0} + (2^2n+0) \binom{2}{1} = \binom{4(\alpha+2n)+0}{4n+0}, \\ \text{(1)} \quad & \alpha \binom{2^2}{0} + (2^2n+1) \binom{2}{1} = \binom{4(\alpha+2n)+2}{4n+1}, \\ \text{(2)} \quad & \alpha \binom{2^2}{0} + (2^2n+2) \binom{2}{1} = \binom{4(\alpha+n+1)+0}{4n+2}, \\ \text{(3)} \quad & \alpha \binom{2^2}{0} + (2^2n+3) \binom{2}{1} = \binom{4(\alpha+n+1)+2}{4n+3}. \end{aligned}$$

Using the identification of subintervals as rectangular regions as discussed in the previous example, our 2- adic lattice is visualized in Fig. 7.

Notice that points of the form $\binom{4(\alpha+2n)+0}{4n+0}$ lie in 0×0 , points of the form $\binom{4(\alpha+2n)+2}{4n+1}$ lie in 2×1 , points of the form $\binom{4(\alpha+n+1)+0}{4n+2}$ lie in 0×2 , and points of the form $\binom{4(\alpha+n+1)+2}{4n+3}$ lie in 2×3 .

4.2.4 Bruhat-Tits Tree and p -adic Lattices

Now that we have developed a method for visualizing p -adic lattices, we would to define the Bruhat-Tits tree in terms of these p -lattices lattices.

Definition: The **Bruhat-Tits** tree is the graph \mathcal{T} with vertices $[\mathcal{L}]$, where $[\mathcal{L}]$ is the

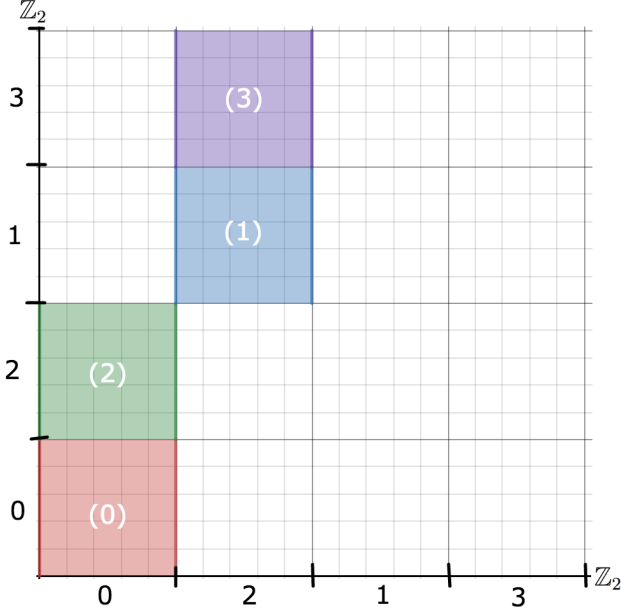


Figure 7: $\text{span}_{\mathbb{Z}_2}\left\{\begin{pmatrix} 2 \\ 1 \end{pmatrix}, \begin{pmatrix} 1 \\ 1 \end{pmatrix}\right\}$

equivalence class of some lattice \mathcal{L} of \mathbb{Q}_p^2 . There is an edge between two vertices a and b of \mathcal{T} if and only if there exists $\mathcal{L}, \mathcal{L}'$ such that

$$a = [\mathcal{L}], b = [\mathcal{L}'], \text{ and } \mathcal{L}' \supset \mathcal{L} \subset p\mathcal{L}. \quad (83)$$

Example 1 and 2 from the previous section were actually the 2-adic lattices that correspond to the vertices 00.0 and 10.0 on \mathcal{T} . To see why this is true, we need to define a coordinate system on \mathcal{T} .

4.2.5 Coordinatizing the Bruhat-Tits Tree

We would like to have a representative pair of vectors for each equivalence class of lattices. Since lattices are equivalent by rescaling and by a change of basis, we are looking for representatives of $\mathbb{Q}_2^* \backslash GL(2, \mathbb{Q}_2) / GL(2, \mathbb{Z}_2)$.

Proposition: For all $M \in PGL(2, \mathbb{Q}_2)$, there exists matrices from

$$\begin{aligned} \bar{N} &\in \left\{ \begin{pmatrix} 1 & 0 \\ x & 1 \end{pmatrix} \mid x \in \mathbb{Z}_2 \right\} \in GL(2, \mathbb{Z}_2), \\ A &\in \left\{ \begin{pmatrix} a_1 & 0 \\ 0 & a_2 \end{pmatrix} \mid a_1, a_2 \in \mathbb{Z}_2 - \{0\} \right\} \in GL(2, \mathbb{Z}_2), \\ N &\in \left\{ \begin{pmatrix} 1 & x \\ 0 & 1 \end{pmatrix} \mid x \in \mathbb{Z}_2 \right\} \in GL(2, \mathbb{Z}_2) \end{aligned}$$

such that

$$M\bar{N}AN = \begin{pmatrix} p^n & a \bmod p^n \\ 0 & 1 \end{pmatrix} =: P.$$

Proof. Begin with an arbitrary $M \in GL(2, \mathbb{Q}_2)$,

$$M = \begin{pmatrix} u_q p^a & u_r p^b \\ u_s p^c & u_t p^d \end{pmatrix}$$

where $u_q, u_r, u_s, u_t \in \mathbb{U}_2$ and a, b, c, d are positive integers.

We can rescale by $p^{-n} \in \mathbb{Q}_2^*$ to clear fractions in one of the entries in the second row. There are two cases to consider

1. If $p^n = p^c$, then $\frac{1}{p^n} \begin{pmatrix} u_q p^a & u_r p^b \\ u_s p^c & u_t p^d \end{pmatrix} = \begin{pmatrix} u_q \frac{p^a}{p^n} & u_r \frac{p^b}{p^n} \\ u_s \frac{p^c}{p^n} & u_t \frac{p^d}{p^n} \end{pmatrix} = \begin{pmatrix} u_q \frac{p^a}{p^n} & u_r \frac{p^b}{p^n} \\ u_s & u_t \alpha \end{pmatrix}$ where $\alpha = p^d/p^n$.
2. If $p^n = p^d$, then $\frac{1}{p^n} \begin{pmatrix} u_q p^a & u_r p^b \\ u_s p^c & u_t p^d \end{pmatrix} = \begin{pmatrix} u_q \frac{p^a}{p^n} & u_r \frac{p^b}{p^n} \\ u_s \frac{p^c}{p^n} & u_t \frac{p^d}{p^n} \end{pmatrix} = \begin{pmatrix} u_q \frac{p^a}{p^n} & u_r \frac{p^b}{p^n} \\ u_s \alpha & u_t \end{pmatrix}$ where $\alpha = p^c/p^n$.

Either case can be chosen without loss of generality since we can always swap the columns of these matrices by $\begin{pmatrix} 0 & 1 \\ 1 & 0 \end{pmatrix}$,

$$\begin{pmatrix} u_q \frac{p^a}{p^n} & u_r \frac{p^b}{p^n} \\ u_s & u_t \alpha \end{pmatrix} \begin{pmatrix} 0 & 1 \\ 1 & 0 \end{pmatrix} = \begin{pmatrix} u_r \frac{p^b}{p^n} & u_q \frac{p^a}{p^n} \\ u_t \alpha & u_s \end{pmatrix}$$

Let's choose case (2). Next, we choose $u_s, u_t = 1 \in \mathbb{U}_2$, so that

$$p^{-n} M = \bar{M} = \begin{pmatrix} u_q \frac{p^a}{p^n} & u_r \frac{p^b}{p^n} \\ \alpha & 1 \end{pmatrix}.$$

Next, we choose a lower triangular matrix from \bar{N} such that

$$\begin{pmatrix} u_q \frac{p^a}{p^n} & u_r \frac{p^b}{p^n} \\ \alpha & 1 \end{pmatrix} \begin{pmatrix} 1 & 0 \\ -\alpha & 1 \end{pmatrix} = \begin{pmatrix} u_r \frac{p^a}{p^n} & u_q \frac{p^b}{p^n} - u_r \alpha \frac{p^b}{p^n} \\ 0 & 1 \end{pmatrix} = \begin{pmatrix} u_r \frac{p^a}{p^n} & \beta \\ 0 & 1 \end{pmatrix}$$

where we have set $\beta = u_q \frac{p^b}{p^n} - u_r \alpha \frac{p^b}{p^n}$.

Then we choose an element from A such that

$$\begin{pmatrix} u_r \frac{p^a}{p^n} & \beta \\ 0 & 1 \end{pmatrix} \begin{pmatrix} u_r^{-1} & 0 \\ 0 & 1 \end{pmatrix} = \begin{pmatrix} \frac{p^a}{p^n} & \beta \\ 0 & 1 \end{pmatrix}.$$

Finally, we choose an element from N such that

$$\begin{pmatrix} \frac{p^a}{p^n} & \beta \\ 0 & 1 \end{pmatrix} \begin{pmatrix} 1 & -y \\ 0 & 1 \end{pmatrix} = \begin{pmatrix} \frac{p^a}{p^n} & \beta - y \frac{p^a}{p^n} \\ 0 & 1 \end{pmatrix} = \begin{pmatrix} \frac{p^a}{p^n} & \gamma \bmod \frac{p^a}{p^n} \\ 0 & 1 \end{pmatrix} = \begin{pmatrix} p^m & \gamma \bmod p^m \\ 0 & 1 \end{pmatrix}.$$

where we set $\frac{p^a}{p^n} = p^m$.

Thus, we have multiplied M by the matrices $\bar{N}AN$ and gotten the matrix

$$P = \begin{pmatrix} p^m & \gamma \bmod p^m \\ 0 & 1 \end{pmatrix}. \tag{84}$$

□

Proposition: For every $M \in PGL(2, \mathbb{Q}_2)$, there exists a unique P .

Proof. Consider two OG matrices

$$A = \begin{pmatrix} p^m & a \\ 0 & 1 \end{pmatrix} \quad \text{and} \quad B = \begin{pmatrix} p^n & b \\ 0 & 1 \end{pmatrix}.$$

There exists a transformations $X \in GL(2, \mathbb{Z}_2)$ such that $AX = B$. Let $X = \begin{pmatrix} x & z \\ y & w \end{pmatrix}$ and choose $y = 0, w = 1$, then

$$\begin{pmatrix} p^m & a \\ 0 & 1 \end{pmatrix} \begin{pmatrix} x & z \\ 0 & 1 \end{pmatrix} = \begin{pmatrix} p^n & b \\ 0 & 1 \end{pmatrix}$$

if and only if $xp^m = p^n$. This implies that $x = p^{m-n}$. To ensure this matrix $X \in GL(2, \mathbb{Z}_2)$, then $m = n$.

□

4.2.6 Choosing a Gauge

We choose a particular representative from the equivalence class of lattices $[\mathcal{L}]$,

$$\begin{pmatrix} p^n & a \bmod p^n \\ 0 & 1 \end{pmatrix} \tag{85}$$

will be called the *Original Gauge* (OG). We will use the span of these column vectors to determine the p -adic lattice to which these coordinates correspond. As a shorthand notation, we will sometimes refer to the coordinate matrices $\begin{pmatrix} p^n & a \bmod p^n \\ 0 & 1 \end{pmatrix}$ as (p^n, a) . We can choose a different representation fro $[\mathcal{L}]$ by multiplying by $\lambda \in \mathbb{Q}_p^*$,

$$\mathcal{L}_1 = \lambda \mathcal{L}_2$$

since two p -adic lattices are equivalent up to rescaling by λ .

4.2.7 Lattices at a Level in the Tree

At level $u = 3$, we have 2^3 vertices in the 2-adic Bruhat-Tits tree. The *OG* coordinate matrices (written in shorthand) for these vertices are

$$(8, 0), (8, 1), (8, 2), (8, 3), (8, 4), (8, 5), (8, 6), (8, 7)$$

and can be visualized in Fig. 15.

The span of these *OG* coordinate matrices are given in the following diagrams.

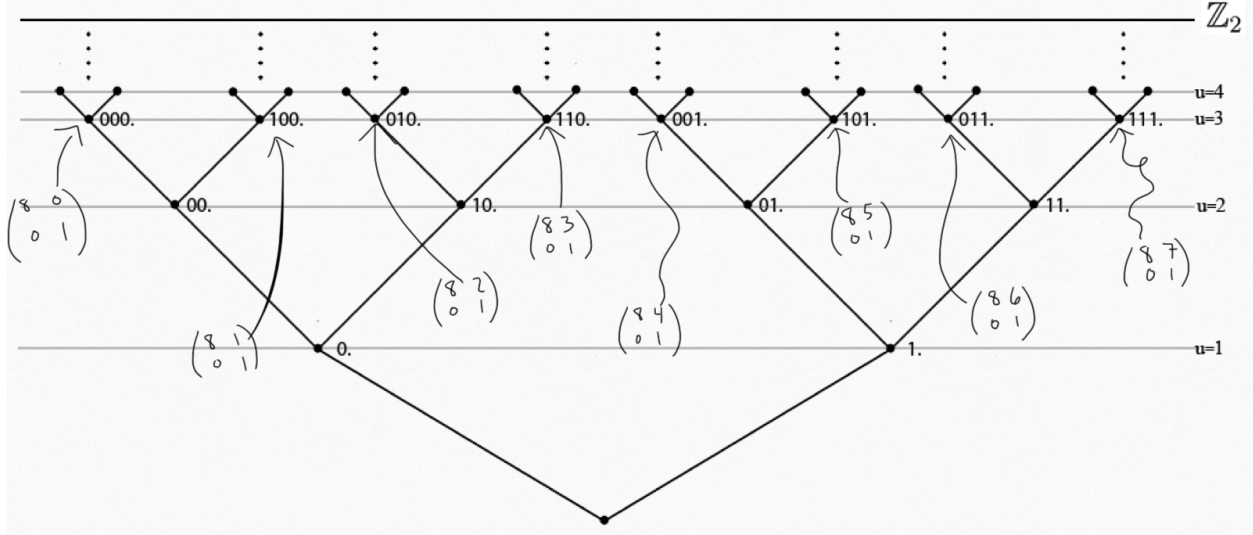


Figure 8: 2-adic Bruhat-Tits tree with OG coordinates labelled at $u = 3$.

These lattices were determined by the following method:

1. $\text{span}_{\mathbb{Z}_2} \left\{ \begin{pmatrix} 2^3 \\ 0 \end{pmatrix}, \begin{pmatrix} 1 \\ 1 \end{pmatrix} \right\}$:

$$\begin{aligned} \alpha \begin{pmatrix} 2^3 \\ 0 \end{pmatrix} + (8n + 0) \begin{pmatrix} 1 \\ 1 \end{pmatrix} &= \begin{pmatrix} 8(\alpha+n)+0 \\ 8n+0 \end{pmatrix}, \\ \alpha \begin{pmatrix} 2^3 \\ 0 \end{pmatrix} + (8n + 1) \begin{pmatrix} 1 \\ 1 \end{pmatrix} &= \begin{pmatrix} 8(\alpha+n)+1 \\ 8n+1 \end{pmatrix}, \\ \alpha \begin{pmatrix} 2^3 \\ 0 \end{pmatrix} + (8n + 2) \begin{pmatrix} 1 \\ 1 \end{pmatrix} &= \begin{pmatrix} 8(\alpha+n)+2 \\ 8n+2 \end{pmatrix}, \\ \alpha \begin{pmatrix} 2^3 \\ 0 \end{pmatrix} + (8n + 3) \begin{pmatrix} 1 \\ 1 \end{pmatrix} &= \begin{pmatrix} 8(\alpha+n)+3 \\ 8n+3 \end{pmatrix}, \\ \alpha \begin{pmatrix} 2^3 \\ 0 \end{pmatrix} + (8n + 4) \begin{pmatrix} 1 \\ 1 \end{pmatrix} &= \begin{pmatrix} 8(\alpha+n)+4 \\ 8n+4 \end{pmatrix}, \\ \alpha \begin{pmatrix} 2^3 \\ 0 \end{pmatrix} + (8n + 5) \begin{pmatrix} 1 \\ 1 \end{pmatrix} &= \begin{pmatrix} 8(\alpha+n)+5 \\ 8n+5 \end{pmatrix}, \\ \alpha \begin{pmatrix} 2^3 \\ 0 \end{pmatrix} + (8n + 6) \begin{pmatrix} 1 \\ 1 \end{pmatrix} &= \begin{pmatrix} 8(\alpha+n)+6 \\ 8n+6 \end{pmatrix}, \\ \alpha \begin{pmatrix} 2^3 \\ 0 \end{pmatrix} + (8n + 7) \begin{pmatrix} 1 \\ 1 \end{pmatrix} &= \begin{pmatrix} 8(\alpha+n)+0 \\ 8n+7 \end{pmatrix}. \end{aligned}$$

Thus the lattice of this span will be the collection of rectangular regions

$$0 \times 0, 1 \times 1, 2 \times 2, 3 \times 3, 4 \times 4, 5 \times 5, 6 \times 6, 7 \times 7$$

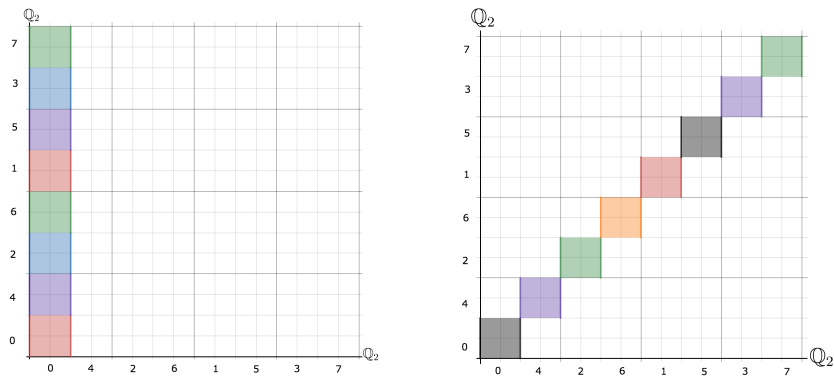


Figure 9: $\text{span}_{\mathbb{Z}_2} \left\{ \begin{pmatrix} 2^3 \\ 0 \end{pmatrix}, \begin{pmatrix} 0 \\ 1 \end{pmatrix} \right\}$ (left) and $\text{span}_{\mathbb{Z}_2} \left\{ \begin{pmatrix} 2^3 \\ 0 \end{pmatrix}, \begin{pmatrix} 1 \\ 1 \end{pmatrix} \right\}$ (right)

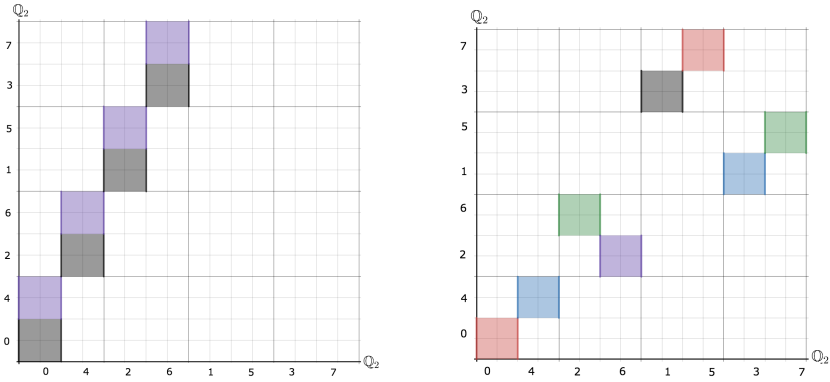


Figure 10: $\text{span}_{\mathbb{Z}_2} \left\{ \begin{pmatrix} 2^3 \\ 0 \end{pmatrix}, \begin{pmatrix} 2 \\ 1 \end{pmatrix} \right\}$ (left) and $\text{span}_{\mathbb{Z}_2} \left\{ \begin{pmatrix} 2^3 \\ 0 \end{pmatrix}, \begin{pmatrix} 3 \\ 1 \end{pmatrix} \right\}$ (right)

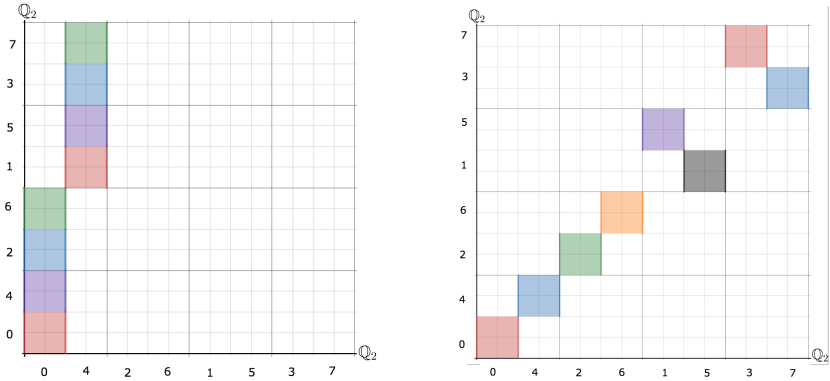


Figure 11: $\text{span}_{\mathbb{Z}_2} \left\{ \begin{pmatrix} 2^3 \\ 0 \end{pmatrix}, \begin{pmatrix} 4 \\ 1 \end{pmatrix} \right\}$ (left) and $\text{span}_{\mathbb{Z}_2} \left\{ \begin{pmatrix} 2^3 \\ 0 \end{pmatrix}, \begin{pmatrix} 5 \\ 1 \end{pmatrix} \right\}$ (right)

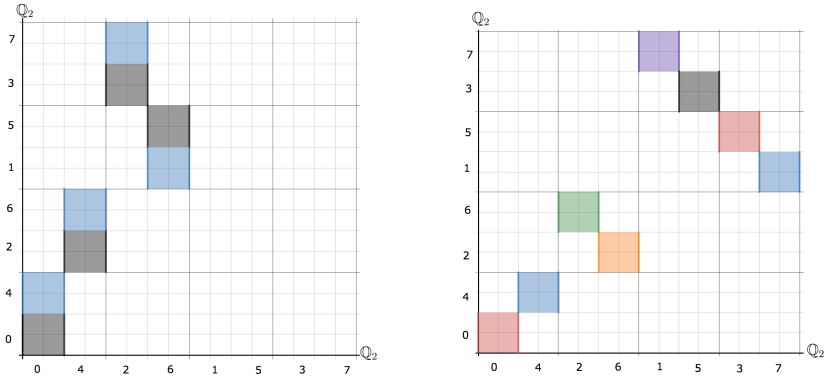


Figure 12: $\text{span}_{\mathbb{Z}_2} \left\{ \begin{pmatrix} 2^3 \\ 0 \end{pmatrix}, \begin{pmatrix} 6 \\ 1 \end{pmatrix} \right\}$ (left) and $\text{span}_{\mathbb{Z}_2} \left\{ \begin{pmatrix} 2^3 \\ 0 \end{pmatrix}, \begin{pmatrix} 7 \\ 1 \end{pmatrix} \right\}$ (right)

2. $\text{span}_{\mathbb{Z}_2} \left\{ \binom{2^3}{0}, \binom{3}{1} \right\}$:

$$\begin{aligned} \alpha \binom{2^3}{0} + (8n+0) \binom{3}{1} &= \binom{8(\alpha+3n)+0}{8n+0}, \\ \alpha \binom{2^3}{0} + (8n+1) \binom{3}{1} &= \binom{8(\alpha+3n)+3}{8n+1}, \\ \alpha \binom{2^3}{0} + (8n+2) \binom{3}{1} &= \binom{8(\alpha+3n)+6}{8n+2}, \\ \alpha \binom{2^3}{0} + (8n+3) \binom{3}{1} &= \binom{8(\alpha+3n+1)+1}{8n+3}, \\ \alpha \binom{2^3}{0} + (8n+4) \binom{3}{1} &= \binom{8(\alpha+3n+1)+4}{8n+4}, \\ \alpha \binom{2^3}{0} + (8n+5) \binom{3}{1} &= \binom{8(\alpha+3n+1)+7}{8n+5}, \\ \alpha \binom{2^3}{0} + (8n+6) \binom{3}{1} &= \binom{8(\alpha+3n+2)+2}{8n+6}, \\ \alpha \binom{2^3}{0} + (8n+7) \binom{3}{1} &= \binom{8(\alpha+3n+2)+5}{8n+7}. \end{aligned}$$

Thus the lattice of this span will be the collection of rectangular regions

$$0 \times 0, 3 \times 1, 6 \times 2, 1 \times 3, 4 \times 4, 7 \times 5, 2 \times 6, 5 \times 7.$$

3. $\text{span}_{\mathbb{Z}_2} \left\{ \binom{2^3}{0}, \binom{7}{1} \right\}$:

$$\begin{aligned} \alpha \binom{2^3}{0} + (8n+0) \binom{7}{1} &= \binom{8(\alpha+7n)+0}{8n+0}, \\ \alpha \binom{2^3}{0} + (8n+1) \binom{7}{1} &= \binom{8(\alpha+7n)+7}{8n+1}, \\ \alpha \binom{2^3}{0} + (8n+2) \binom{7}{1} &= \binom{8(\alpha+7n+1)+6}{8n+2}, \\ \alpha \binom{2^3}{0} + (8n+3) \binom{7}{1} &= \binom{8(\alpha+7n+2)+5}{8n+3}, \\ \alpha \binom{2^3}{0} + (8n+4) \binom{7}{1} &= \binom{8(\alpha+7n+3)+4}{8n+4}, \\ \alpha \binom{2^3}{0} + (8n+5) \binom{7}{1} &= \binom{8(\alpha+7n+4)+3}{8n+5}, \\ \alpha \binom{2^3}{0} + (8n+6) \binom{7}{1} &= \binom{8(\alpha+7n+5)+2}{8n+6}, \\ \alpha \binom{2^3}{0} + (8n+7) \binom{7}{1} &= \binom{8(\alpha+7n+6)+1}{8n+7}. \end{aligned}$$

Thus the lattice of this span will be the collection of rectangular regions

$$0 \times 0, 7 \times 1, 6 \times 2, 5 \times 3, 4 \times 4, 3 \times 5, 2 \times 6, 1 \times 7.$$

The other spans can be calculated using the same process.

4.2.8 Action of $PGL(2, \mathbb{Z}_2)$ on \mathcal{T}_2

Every semisimple Lie group can be decomposed using the Iwasawa decomposition into a product of an orthogonal matrix and an upper triangular matrix (ref). For instance, if our group is $SL(2, \mathbb{R})$, then we can take

$$K = \left\{ \begin{pmatrix} \cos \theta & -\sin \theta \\ \sin \theta & \cos \theta \end{pmatrix} \right\}, \quad A = \left\{ \begin{pmatrix} a & 0 \\ 0 & a^{-1} \end{pmatrix} \mid a \neq 0 \right\}, \quad N = \left\{ \begin{pmatrix} 1 & x \\ 0 & 1 \end{pmatrix} \right\}.$$

So any matrix $M \in SL(2, \mathbb{R})$ can be decomposed into a product of matrices,

$$M = KAN.$$

This decomposition works well over an Archimedean field such as \mathbb{R} , but the notion of rotation matrices isn't as well-defined for non-Archimedean fields such as \mathbb{Q}_p . This is why we must consider the Non-Archimedean Iwasawa decomposition if we would like to decompose matrices in $PGL(2, \mathbb{Q}_p)$.

Proposition: Any matrix $M \in PGL(2, \mathbb{Q}_2)$ can be written as the product, $M = KAN$, of the maximal subgroup $K = PGL(2, \mathbb{Z}_2)$ and upper triangular matrices,

$$A = \left\{ \begin{pmatrix} a & 0 \\ 0 & a^{-1} \end{pmatrix} \mid a \neq 0 \right\}, \quad N = \left\{ \begin{pmatrix} 1 & x \\ 0 & 1 \end{pmatrix} \right\}.$$

4.2.9 Right Multiplication by $PGL(2, \mathbb{Z}_2)$

Right multiplication by an element of $PGL(2, \mathbb{Z}_2)$ is just a change of basis over \mathbb{Z}_2 . This does not change the \mathbb{Z}_2 -span of any two vectors. Thus, 2-adic lattices are invariant under right action of $PGL(2, \mathbb{Z}_2)$.

$$\begin{pmatrix} p^n & a \bmod p^n \\ 0 & 1 \end{pmatrix} \begin{pmatrix} m & n \\ s & t \end{pmatrix} = \begin{pmatrix} p^n \cdot m & a \cdot s \\ s & t \end{pmatrix}$$

Additionally, rescaling by powers of 2 give equivalent lattices since equivalence classes of

$$\mathcal{L} \sim \mathcal{L}' \iff \mathcal{L} = \lambda \mathcal{L}' \text{ where } \lambda \in \mathbb{Q}_p^*.$$

4.2.10 Left Multiplication by $PGL(2, \mathbb{Z}_2)$

We are able to move around the tree by left multiplication of matrices from $PGL(2, \mathbb{Z}_2)$.

Example 4.3. Say we begin at the coordinate $(2^2, 0)$ and would like to find the transformation that takes us to $(2^2, 1)$, then

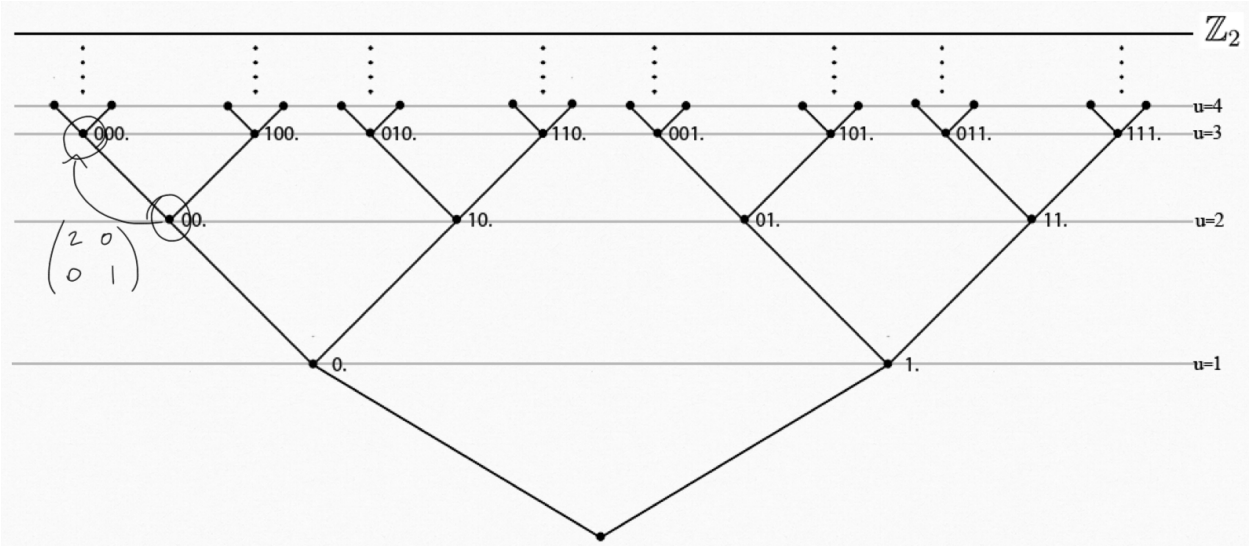
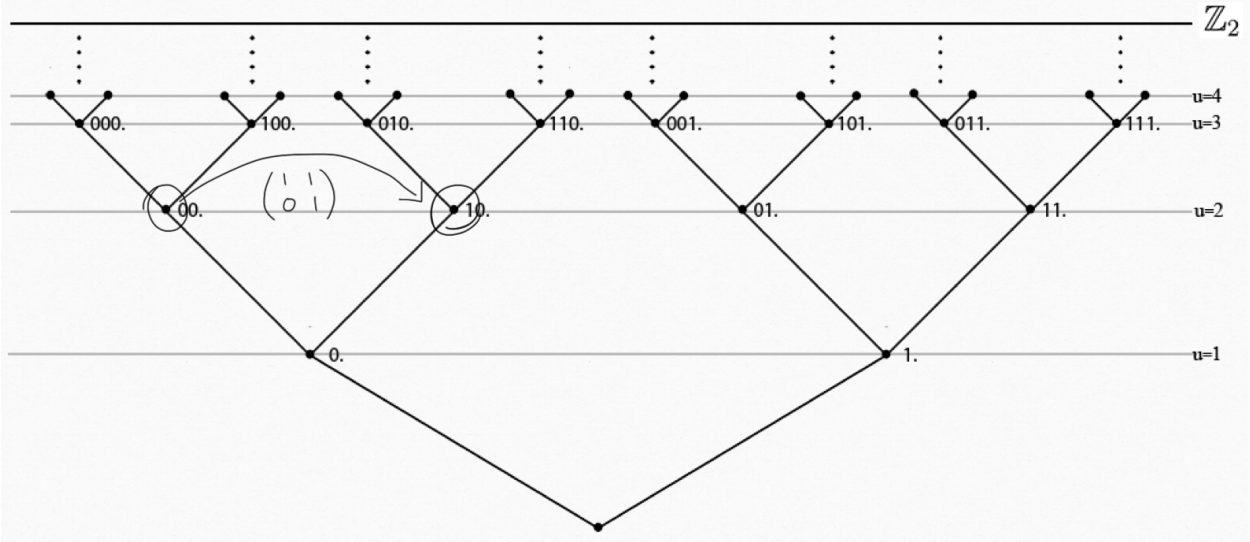
$$\begin{pmatrix} a & b \\ c & d \end{pmatrix} \begin{pmatrix} 2^2 & 0 \\ 0 & 1 \end{pmatrix} = \begin{pmatrix} 2^2 & 0 \\ 0 & 1 \end{pmatrix} \iff a = b = d = 1, c = 0.$$

Therefore, the matrix $\begin{pmatrix} 1 & 1 \\ 0 & 1 \end{pmatrix}$ takes $(2^2, 0) \mapsto (2^2, 1)$.

Example 4.4.

$$\begin{pmatrix} a & b \\ c & d \end{pmatrix} \begin{pmatrix} 2^2 & 0 \\ 0 & 1 \end{pmatrix} = \begin{pmatrix} 2^3 & 0 \\ 0 & 1 \end{pmatrix} \iff a = 2, b = c = 0, d = 1.$$

Therefore, the matrix $\begin{pmatrix} 2 & 0 \\ 0 & 1 \end{pmatrix}$ takes $(2^2, 0) \mapsto (2^3, 0)$.



Example 4.5.

$$\begin{pmatrix} a & b \\ c & d \end{pmatrix} \begin{pmatrix} 2^2 & 0 \\ 0 & 1 \end{pmatrix} = \begin{pmatrix} 2^3 & 6 \\ 0 & 1 \end{pmatrix} \iff a = 2, b = 6, c = 0, d = 1.$$

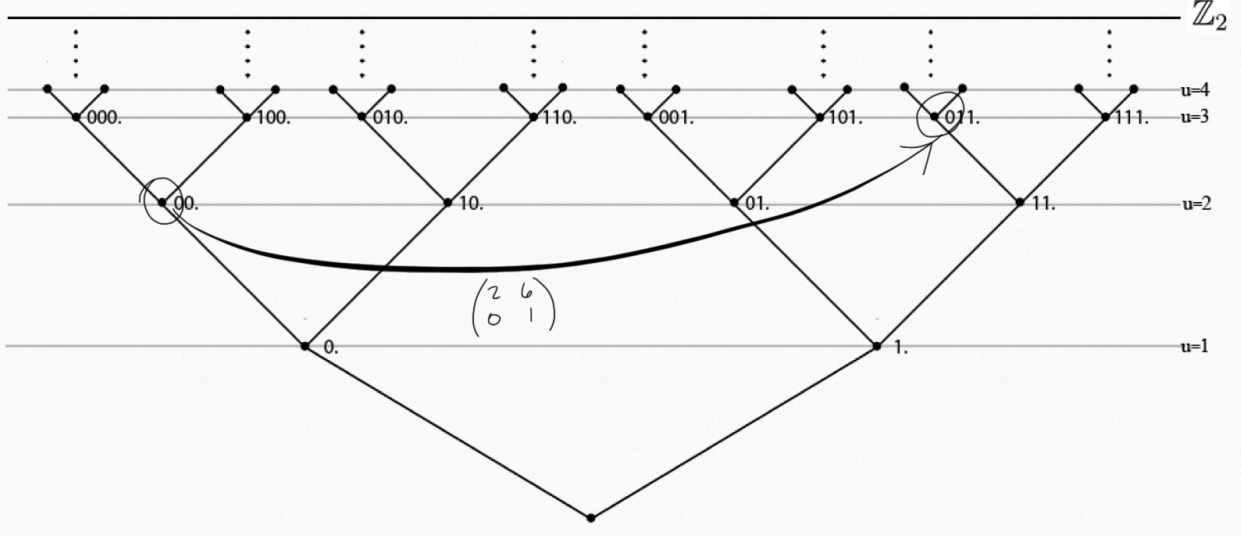
Therefore, the matrix $\begin{pmatrix} 2 & 6 \\ 0 & 1 \end{pmatrix}$ takes $(2^2, 0) \mapsto (2^3, 6)$.

Theorem 4.3. The group $GL(2, \mathbb{Z}_2)$ acts transitively on \mathcal{T}_2 by left multiplication.

Proof. Consider the vertices A and B in the tree given by OG matrices $A = \begin{pmatrix} p^m & a \bmod p^m \\ 0 & 1 \end{pmatrix}$ and $B = \begin{pmatrix} p^n & b \bmod p^n \\ 0 & 1 \end{pmatrix}$. We can left multiply A by $\begin{pmatrix} p^{n-m} & \alpha \\ 0 & 1 \end{pmatrix} \in GL(2, \mathbb{Z}_2)$,

$$\begin{pmatrix} p^{n-m} & \alpha \\ 0 & 1 \end{pmatrix} \begin{pmatrix} p^m & a \bmod p^m \\ 0 & 1 \end{pmatrix} = \begin{pmatrix} p^n & p^{n-m}a \bmod p^m - \alpha \\ 0 & 1 \end{pmatrix} \iff \alpha = b \bmod p^n.$$

Thus, $GL(2, \mathbb{Z}_2)$ acts transitively on \mathcal{T}_2 . □



4.2.11 Constructing the Bruhat-Tits Tree as a Coset Space

We have shown that once we have chosen a representative from OG , we can multiply these coordinate matrices by elements of $PGL(2, \mathbb{Q}_2)$ to move around in the tree. This implies that $PGL(2, \mathbb{Q}_2)$ acts transitively on the tree. We also note that the maximal compact subgroup of $PGL(2, \mathbb{Q}_2)$ is $PGL(2, \mathbb{Z}_2)$. Using this fact and theorem 4.1, we can construct the coset space

$$\mathcal{T}_2 := PGL(2, \mathbb{Q}_2)/PGL(2, \mathbb{Z}_2). \quad (86)$$

4.3 \mathcal{T}_2 as a Discrete Analog of AdS_2

4.3.1 $SO(2, 1) \approx SL(2, \mathbb{R})$

In the previous section, we viewed AdS_2 as the coset space

$$AdS_2 = SO(2, 1)/SO(1, 1). \quad (87)$$

Our goal in this section is to relate (87) to the Bruhat-Tits tree which is the coset space

$$\mathcal{T}_2 = PGL(2, \mathbb{Q}_2)/PGL(2, \mathbb{Z}_2).$$

To do this, we need to relate the group $SO(2, 1)$ to $PGL(2, \mathbb{Q}_2)$. At first glance this seems difficult because the notion of p -adic orthogonal matrices is not well-defined. This is because the usual real rotation matrices contain cosines and sines, which are not p -adic valued functions. To circumvent this problem, we look at the isomorphism

$$SO(2, 1) \approx SL(2, \mathbb{R})$$

where \approx denotes the relation on Lie groups where some realization of their Lie algebras are isomorphic.

Proposition: $SO(2, 1) \approx SL(2, \mathbb{R})$.

Proof. Consider the basis $\{J_x, J_y, J_z\}$ of $so(3, \mathbb{R})$ where

$$J_x = \begin{pmatrix} 0 & 0 & 0 \\ 0 & 0 & 1 \\ 0 & 1 & 0 \end{pmatrix}, \quad J_y = \begin{pmatrix} 0 & 0 & -1 \\ 0 & 0 & 0 \\ 1 & 0 & 0 \end{pmatrix}, \quad J_z = \begin{pmatrix} 0 & 1 & 0 \\ 1 & 0 & 0 \\ 0 & 0 & 0 \end{pmatrix}.$$

Then there exists an isomorphism $\phi: so(3, \mathbb{R}) \rightarrow sl(2, \mathbb{R})$ defined by

$$J_x \mapsto -\frac{i}{2}(J_+ + J_-), \quad J_y \mapsto \frac{1}{2}(J_- - J_+), \quad J_z \mapsto -\frac{i}{2}h$$

where (J_+, J_-, h) is a basis for $sl(2, \mathbb{R})$ given by

$$J_+ = \begin{pmatrix} 0 & 1 \\ 0 & 0 \end{pmatrix}, \quad J_- = \begin{pmatrix} 0 & 0 \\ 1 & 0 \end{pmatrix}, \quad h = \begin{pmatrix} 1 & 0 \\ 0 & -1 \end{pmatrix}.$$

□

Now that we have related $SO(2, 1)$ to $SL(2, \mathbb{R})$, we replace $SO(2, 1)$ with $SL(2, \mathbb{R})$ in the coset construction of AdS_2 to get the space

$$SL(2, \mathbb{R})/SO(2). \tag{88}$$

This coset space is the interior of the upper half plane \mathbb{H} . We note that the boundary of \mathbb{H} is \mathbb{R} . The space (88) has a natural $SL(2, \mathbb{R})$ -invariant hyperbolic metric. The interior of \mathbb{H} is noncompact with respect to this metric, but can be compactified by adding points at infinity.

This is where p -adics comes into play. We now replace $SL(2, \mathbb{R})$ with its p -adic counterpart $GL(2, \mathbb{Q}_2)$ and replace the maximal compact subgroup $SO(2)$ with $GL(2, \mathbb{Z}_2)$. Then modding out by scalar transformations from \mathbb{Q}_p^* results in the coset space

$$\mathcal{T}_2 = PGL(2, \mathbb{Q}_2)/PGL(2, \mathbb{Z}_2). \tag{89}$$

The geodesics in both \mathcal{T}_2 and AdS_2 are very similar, where \mathcal{T}_2 is equip with the p -adic metric and AdS_2 is equip with the usual hyperbolic metric. In \mathcal{T}_2 , the geodesics between points a and b on the boundary \mathbb{Q}_2 follow geodesics as depicted in Fig. 16. In AdS_2 , the geodesics between points a and b on the boundary \mathbb{R} follow semicircular paths as depicted in Fig. 16.

This completes the analogy between the Bruhat-Tits tree \mathcal{T}_2 and Anti de Sitter space AdS_2 .

5 Conclusion and Future Work

5.1 Conclusion

In section 2, we saw when examining the Eternal Symmetree model that the p -adic numbers are useful tools in models that have an inherently hierarchical structure. The p -adics allowed us to uniquely describe points on the boundary of the tree and allowed us to see the conformal

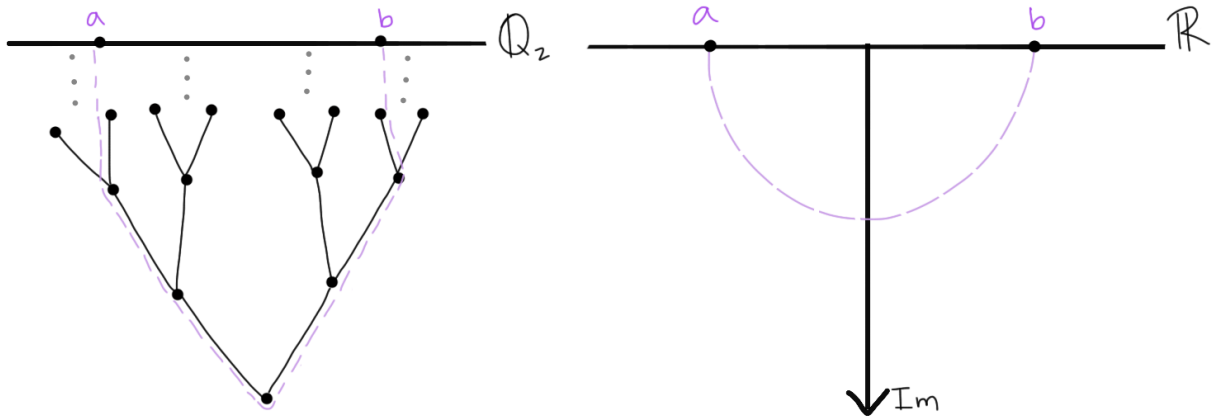


Figure 16: The dotted line represents the geodesics between points on the boundary of \mathcal{T}_2 and AdS_2 .

symmetries of the tree. The two-point correlation functions that we computed in this section depended explicitly on a p -norm. In this section we also studied how multifractal measures on the boundary of the tree arise when in the presence of terminal vacuums. This correlation function also depended explicitly on a p -adic norm.

In section 3, we examined how the p -adic numbers facilitate a construction for an algebra of observables. That is, the Bruhat-Tits tree has finite strings of digits on which operators act and this operator algebra serves as observables. From here we were able to follow the construction presented in [3] to formulate a quantum mechanical Eternal Symmetree model.

Finally, in the last section we discussed p -adic Anti-De Sitter space. We first constructed AdS as a coset space and then constructed the Bruhat-Tits tree as a coset space. To do this, we formulated a new way to visualize p -adic lattices in \mathbb{Q}_2^2 . We determined the left action of $PGL(2, \mathbb{Z})$ on original gauge matrices and used this to move between vertices in the tree.

5.2 Future Work

In the future, I would like to understand the p -adic AdS/CFT correspondence presented in [14]. The work done in my paper focuses on only one half of the correspondence. That is, I focused on understanding AdS space as a coset space and on the analogy between the Bruhat-Tits tree and AdS. However, the world of conformal field theories is one that I would like to understand in the future. In [14], the authors only explore scalar field theories on the Bruhat-Tits tree and I would like to eventually formulate spinor field theories on the Bruhat-Tits tree.

In [4], it is shown that the Bruhat-Tits tree is an analog of the open string world sheet and the author constructs a lattice quantum field theory on the Bruhat-Tits tree with a simple local Lagrangian. The lattice constructed in this paper is more of an \mathbb{Z} -lattice in \mathbb{Q}^2 rather than a \mathbb{Z}_p -lattice in \mathbb{Q}^2 . I would like to see if I can incorporate the \mathbb{Z}_p -lattices constructed in my paper to this paper on non-Archimedean string theories.

Another goal is to look at 2-adic lattices at levels higher than $u = 3$. I believe there is

a combinatorial interpretation for the way the blocks arrangement themselves and would like to understand the ways these 2-adic lattices change when moving up levels in the tree. Additionally, I would like to understand how 2-adic lattices compare to their 3-adic counterparts.

5.3 Acknowledgements

The last 50 pages would not have been possible without the guidance of my thesis advisor, David Cherney. I took Cherney’s introduction to proof-writing class the very first quarter I transferred to UC Davis. One day during office hours for his class, I mentioned to him that I was interested in understanding how group theory gets involved in quantum mechanics. I didn’t expect that comment to lead to nearly two years of work culminating in a senior thesis.

Working with him on this project has been the highlight of my undergraduate education and I’m incredibly grateful that he has dedicated so much time and put up with me for two years.

Also, by writing this acknowledgements paragraph and including the references to the total page count (because I can), my senior thesis is officially longer than Cherney’s senior thesis... so take that Cherney.

6 References

- [1] Guth, Alan H. 2007. “Eternal inflation and its Implications.” *Journal of Physics A: Mathematical and Theoretical* 40: 6811–6826. [arXiv:hep-th/0702178].

- [2] D. Harlow, S. H. Shenker, D. Stanford, and L. Susskind, “Eternal Symmetree,” *Phys. Rev. D* 85, 063516 (2012) [arXiv:1110.0496 [hep-th]].

- [3] Marcolli M., Tedeschi N., “Multifractals, Mumford Curves and Eternal Inflation”, [arXiv:1311.5458].

- [4] A. Zabrodin, , “Non-archimedean string action and Bruhat-Tits trees,” *Comm. Math. Phys.* 123, 463-483 (1989).

- [5] L. Susskind, “Fractal-Flows and Time’s Arrow,” arXiv:1203.6440 [hep-th].

- [6] J. Fröhlich, B. Schubnel, “Quantum Probability Theory and the Foundations of Quantum Mechanics,” arXiv:1310.1484 [quant-ph].

- [7] J. Cuntz, W. Krieger, “A Class of C^* -Algebras and Topological Markov Chains,” *Inventiones mathematicae* 251-268, vol.56 (1980).
- [8] Bratteli O, Robinson DW (1981, 1997) *Operator algebras and quantum statistical mechanics 2. Equilibrium states. Models in quantum statistical mechanics.* Springer Verlag, Berlin–Heidelberg–New York.
- [9] M. Kesseböhmer, M. Stadlbauer, B. O. Stratmann, “Radon–Nikodym representations of Cuntz–Krieger algebras and Lyapunov spectra for KMS states,” *Mathematische Zeitschrift* 256, no. 4, 871-893 (2007), arXiv:math/0601354 [math.DS].
- [10] A.M. Robert (2000) “A Course in p -adic Analysis,” *The Compact Space \mathbb{Z}_p ,* Springer-Verlag, Berlin–Heidelberg–New York.
- [11] Neal Koblitz (1984) “ p -adic Numbers, p -adic Analysis, and Zeta-Functions” Springer-Verlag, Berlin–Heidelberg–New York.
- [12] Leonard Susskind (2014) “Aspects of Eternal Inflation” *Lecture Series at Stanford University.*
- [13] Alex Kumjian, David Pask, Iain Raeburn. “Cuntz-Krieger algebras of directed graphs”
- [14] Steven S. Gubser, Johannes Knaute, Sarthak Parikh, Andreas Samberg, and Przemek Witaszczyk. “ p -adic AdS/CFT” arXiv:1605.01061v2 [hep-th]